On-demand analogue spacetime in superconducting networks: Grey holes, dynamical instability and exceptional points

Mohammad Atif Javed[⋆], Daniel Kruti, Ahmed Kenawy, Tobias Herrig[†], Christina Koliofoti, Oleksiy Kashuba[‡] and Roman-Pascal Riwar

Peter Grünberg Institute, Theoretical Nanoelectronics,
Forschungszentrum Jülich, D-52425 Jülich, Germany

⋆ atif4598@gmail.com

Abstract

There has been considerable effort to mimic analogue black holes and wormholes in solid state systems. Lattice realisations in particular present specific challenges. One of those is that event horizons in general have both white and black hole (grey hole) character, a feature guaranteed by the Nielsen-Ninomiya theorem. We here explore and extend the capability of superconducting circuit hardware to implement on-demand spacetime geometries on lattices, combining the nonreciprocity of gyrators with the non-linearity of Josephson junctions. We demonstrate the possibility of the metric sharply changing within a single lattice point, thus entering a regime where the modulation of system parameters is "trans-Planckian", and the Hawking temperature ill-defined. Instead of regular Hawking radiation, we find an instability in the form of an exponential burst of charge and phase quantum fluctuations over short time scales – a robust signature even in the presence of an environment. Moreover, we present a loop-hole for the typical black/white hole ambiguity in lattice simulations: exceptional points in the dispersion relation allow for the creation of pure black (or white) hole horizons, at the expense of a radical change in the dynamics of the wormhole interior.

Copyright M. A. Javed *et al*.
This work is licensed under the Creative Commons
Attribution 4.0 International License.
Published by the SciPost Foundation.

Received 2025-08-28
Accepted 2026-02-02
Published 2026-02-17
doi:10.21468/SciPostPhys.20.2.047

Check for updates

Contents

1 Introduction **2**

2 Curved space time metrics and the circuit simulator **4**
2.1 Brief review of field theories with curved spacetime and stability considerations 4
2.2 Simulation with circuit networks 7

3 Setup **11**

4 Realising negative inductance through quench **17**

[†] Current address: Institute for Quantum Materials and Technology, Karlsruhe Institute of Technology, 76131 Karlsruhe, Germany.
[‡] Current address: Institute for Quantum Information, RWTH Aachen University, 52074 Aachen, Germany.

5 Analogue horizons via flux quench 21

6 Perspective on wormhole evaporation over long times 26

7 Conclusions and outlook 27

A Josephson junction array with gyrators 28

B Bogoliubov transformation for calculating correlations after quench 31

C Klich's determinant formula 33

D Correlation matrix from Klich's determinant formula 36

E Hawking-Unruh radiation on a lattice 38

F Effect of disorder 42

References 47

1 Introduction

Unifying quantum mechanics and gravity poses several theoretical [1–3] and experimental challenges [4–14], which motivates studying analogues of relativistic quantum effects in experimentally accessible systems [15]. Several ideas have therefore been proposed for simulating gravitational effects in solid-state systems – for example, holographic ideas borrowed from string theory [16–21], or cosmological particle creation [22–27], or more directly, using Unruh's proposal of "sonic black holes" [28] as an inspiration to simulate black holes in labs. Along these lines, apparent event horizons and the resulting Hawking radiation have been studied on various platforms [29–37], most notably in ultracold atomic gases [38–42].

There remain however a number of open questions. First, so far for solid state implementations the metric usually changes only over a finite "healing length". If the surface gravity (for analogue black holes surface gravity corresponds to the rate of change of the group velocity with which a signal will move in the given metric [41]) is too weak, the resulting small Hawking temperature may thus be below the threshold of the system's intrinsic temperature [43] – an obstacle that (at least up to now) seems to have only been overcome for cold atom simulators [41]. Relatedly, systems with an apparent event horizon generically do not have a well-defined ground state, such that any coupling to the environment leads to an instability, making it extremely challenging to distinguish intrinsic radiation due to the horizon (which would actually simulate aspects of a universe with nontrivial spacetime metric) and radiation due to environment induced relaxation. In addition, even in the absence of environment, the closed system can in some platforms be spontaneously unstable [38, 39]. Furthermore, lattice realisations (which ultimately concerns all solid state systems) add a number of interesting but challenging facets, such as a natural (though possibly artifical) resolution of the trans-Planckian problem [44–47], and most notably, the fact that any event horizon has both black and white hole character (also referred to as grey hole), since the dispersion relation in a periodic Brillouin zone must necessarily cross zero at least twice [31], a simple consequence of the Nielsen-Ninomiya theorem [48].

Superconducting circuits are one of the prime candidates for building large-scale quantum hardware [49–51]. The behaviour of these circuits and their interactions with quantised electromagnetic fields in the microwave range are described by circuit quantum electrodynamics (cQED), a formalism that reduces circuits to lumped elements whose phase and charge are canonically conjugate [52–60]. The toolbox of superconducting circuits includes nonlinear elements such as Josephson junctions and linear elements such as capacitors and inductors. Our work will also feature nonreciprocal multi-port circuit elements. Classical nonreciprocal elements called gyrators (or their close cousins, circulators), are already widely in use in circuit engineering and signal processing [61–64], whose consistent circuit theoretical description goes back to the work by Tellegen [65]. These are however generally large clunky objects operating in a finite frequency window. Various recent works strive towards a realisation and a consistent description of quantum mechanical gyrators [66–69]. Moreover, it has recently been realised [69–72] that the same nonreciprocal behaviour also occurs due to topological transitions in the transport degrees of freedom of multiterminal junctions [73–81], whose size can be on the meso scale and the gyration behavior emerges in the dc limit.

Over the course of decades, it has been shown that networks of superconducting circuits can give rise to a large number of physical phenomena and imitate various quantum field theories from other domains [34,82–94]. However, the exploration of analogue gravity phenomena has so far been limited to Hawking-like radiation in Josephson junction arrays [32–35,95–98], which, due to the nature of their proposal leave only little control over the shape of the spacetime geometry, or recreation of a limited class of curved spacetimes by means of flux control of SQUID arrays [36,37].

In this work, we demonstrate that networks of Josephson junctions and gyrators can be used as an engineering tool for simulations of quantum-gravity phenomena with unprecedented tunability capabilities, and generate surprising insights specific to lattice systems. The basic idea is that arrays of these elements result in a (nearly) massless scalar field theory describing a quantum field – the superconducting phases of the charge islands – propagating across a lattice with spatially varying analogue spacetime metric. Contrary to effective modulations of spacetime (metric) by the excitation of solitons [98] in superconducting circuits, here a nontrivial spacetime and event horizons emerge via direct parametric control of the gyration and induction values of the circuit elements within the network. The local analogue spacetime metric essentially encompasses the local dispersion relation, i.e., the velocities with which right and left signals move with respect to the laboratory frame.

To create an apparent horizon we need a boundary between the "normal region" (region where the signals can move in both directions) and a wormhole region where the signals only move in one direction, i.e., a region with overtilted dispersion relation. As it turns out such a region can be created with *negative* inductors, which we propose to achieve by adapting recent insights in flux quench of regular Josephson junctions [60,99]. Tunable $0-\pi$ junctions [100–102] may offer an alternative pathway towards negative inductances.

Already for such classical metric profiles, we make a number of important observations specific to lattice simulations. The exceptional tunability of the individual energy scales in the lattice allows to change the analogue metric over only a few lattice sites, which would yield for typical charging and Josephson energies Hawking temperatures in the 100mK up to $1K$ range, thus comfortably exceeding usual cryogenic temperatures. But as we show, this comes at the price of a fundamental impossibility to create stable event horizons for strictly discrete lattice systems. Instead, the system becomes unstable right after the quench, resulting in an immediate evaporation starting out from the event horizon. We show that the instability leads to an accumulation of charge and phase quantum fluctuations, which we expect to be a highly robust signature with respect to environment-induced dissipation, since the latter *reduces* quantum fluctuations (instead of increasing them). Moreover, we find an instructive

loop-hole to the aforementioned ambiguity of black- versus white hole event horizons in lattice systems. Namely, the inductive coupling can go either via nearest or next-to-nearest neighbour nodes. For the former, the dispersion relation inside the wormhole region exhibits an *exceptional point* (EP), such that the eigenspectrum no longer crosses zero energy twice, but instead takes a detour on the complex plane to satisfy periodicity. We thus realise lattice versions of event horizons which are definitely either black- or white hole, but not both. However, this feature radically changes the dynamics in the interior of the wormhole: instead of an evaporation from the horizons outwards the entire wormhole interior evaporates everywhere immediately after the quench. Our work thus connects to the currently highly active research field dealing with EPs, generic topological defects in non-Hermitian matrices [103]. EPs have been studied in various areas of physics such as optics [104, 105], acoustics [106] and quantum mechanics [107–109]. They also play an important role in condensed matter systems described by non-Hermitian Hamiltonians [110–112], specifically as a basis for their topological properties [113–117]. In our work the non-Hermitian matrix (and EPs) arise due to bosonic Bogoliubov transformations. We will go into a little more detail about complex eigenvalues as we encounter them, but in short this is due to the fact that the Bogoliubov transformations for bosons are symplectic, unlike fermions where the transformations are unitary. Furthermore, while we consider long chains in the main part of this work, as they provide a clean interpretation of the effects in the context of curved spacetime, we are aware that they may be challenging to realise experimentally. Therefore in the outlook, we propose experiments on only few lattice points as proofs of principle, which already contain much of the pertinent phenomenology present in long chains.

The prediction of both astrophysical and analogue event horizons is predicated on the semi-classical approximation, i.e. quantum field theory on fixed background spacetime. Our work here provides a first step towards investigating the backaction of quantum fields on spacetime, as should be clear from our discussion in Sec. 6, where we qualitatively consider the long-term effect of decaying event horizons in our system. However, this point needs further investigation in future with some concrete calculations, possibly with a simplified model of the effect of evolving quantum fields on spacetime. We have planned a manuscript in the future with one possible realisation of this idea in superconducting circuits using multi-stable JJs [118–120].

This paper is organized as follows. Sec. 2 is a brief review of scalar field theories on curved spacetime, and a summary of our main accomplishments of this work. In Sec. 3 we introduce and study the two circuits that will host the apparent horizons that we wish to investigate, we especially focus on the different effect that negative inductances have on the dispersion relations of these two circuits anticipating the differences between the horizons in them. Sec. 4 is a brief detour, where we expand upon the idea of using flux quench on a Josephson junction to get a negative inductance, and in Sec. 5 we study and characterise the horizons in the two aforementioned circuits, by looking at the time evolution of quantum fluctuations of the conjugate charge and the phase difference. In Sec. 6 we hypothesise on the long time fate of the analogue horizons and argue that the effect of this intrinsic evaporation is easily distinguishable from the effect of coupling to the environment.

2 Curved space time metrics and the circuit simulator

2.1 Brief review of field theories with curved spacetime and stability considerations

To set the stage, let us reiterate basic notions related to field theories with nontrivial spacetime metric.

Within this brief review, questions regarding the stability of the considered systems will emerge. To this end, we begin by providing a number of general statements regarding bosonic Hamiltonians (as we focus on scalar bosonic quantum fields). The quantum systems we consider are all described by a Hermitian Hamiltonian. In accordance with Refs. [38,39,121,122], we point out that hermiticity does *not* guarantee stability of the system, due to the special symplectic structure of the Bogoliubov transformation. In particular, two cases need to be distinguished. It may happen that certain eigenvalues are negative, such that the system has no well-defined many-body ground state. Such systems however still evolve in a stable fashion, unless they are coupled to an environment, which will in general lead to a collapse of the system, as negative energy bosonic states can now be occupied by extracting energy from the bath. In the second case, some eigenenergies may become *complex* (again, this is consistent with Hermitian Hamiltonians, see Refs. [38, 39]). Such systems are spontaneously unstable, as they do not require a coupling to a bath to collapse.

In continuous field theories, the action of a field ϕ in a $d+1$-dimensional spacetime is generally given as

$$S = \frac{1}{2}\int dt d^d x \sqrt{-g}\, g^{\mu\nu}\partial_\mu\phi\, \partial_\nu\phi\,, \tag{1}$$

where the metric tensor $g^{\mu\nu}$ can in general depend on all coordinates. Within actual general relativity, the metric tensor of course encompasses the entire causal structure of spacetime. However, it is understood since a long time that a wide variety of nonrelativistic systems (condensed matter and beyond) may be described by an action of the same form, however with typical velocities much below the speed of light (see, e.g., acoustic phonons [123], plasmon excitations in Luttinger liquids [124], or charge waves in Josephson junction arrays [90]). These systems provide an analogue spacetime in the sense that $g^{\mu\nu}$ looses its concrete relativistic interpretation.

For simplicity, let us consider $1+1$ dimensions (note that our simulator recipe works also for more spatial dimensions, as we point out in a moment), and focus on metrics that depend only on the position coordinate, i.e., metrics that are stationary in the laboratory frame. Here we write the action explicitly in a matrix form as

$$S = \frac{1}{2}\int dt dx \begin{pmatrix} \partial_t\phi & \partial_x\phi \end{pmatrix} \begin{pmatrix} \frac{1}{u} & \frac{v}{u} \\ \frac{v}{u} & \frac{v^2-u^2}{u} \end{pmatrix} \begin{pmatrix} \partial_t\phi \\ \partial_x\phi \end{pmatrix}, \tag{2}$$

where u and v are two independent functions of x. Note that the matrix representing the spacetime metric has determinant -1, such that the $\sqrt{-g}$ prefactor is here irrelevant.[1] For actions of this form, it is always possible to make a coordinate transformation [43]

$$y = t - \int^x dx' \frac{1}{u(x')+v(x')}, \tag{3}$$

$$z = t + \int^x dx' \frac{1}{u(x')-v(x')}, \tag{4}$$

to bring the action into the simple form

$$S = \int dy dz \partial_y\phi\, \partial_z\phi\,. \tag{5}$$

[1] This action breaks the time reversal symmetry (TRS) due to non-zero v. This breaking of TRS is unavoidable in most proposals for apparent event horizons as the basic goal is to recreate the Painlevé–Gullstrand–Lemaître metric described in Ref. [43]. As far as astrophysical event horizons are concerned, equations of General Relativity are invariant under TRS, but their macroscopic consequences such as an accretion disk are not time reversible. In addition, the time reversed black hole solutions are the white hole solutions, which have so far not been observed in our universe.

In these coordinates, the classical Euler-Lagrange equation is simply $\partial_y \partial_z \phi = 0$, whose solutions are arbitrary superpositions of functions that depend either only on y, or only on z. Transforming back to (t, x)-coordinates via Eqs. (3) and (4), these two separate solutions correspond to waves propagating locally either with velocity $u+v$ or $u-v$. For constant u, v (and $u > 0$), the theory is readily quantised, yielding the Hamiltonian

$$H = \int dk \omega_k a_k^\dagger a_k \,, \tag{6}$$

where for bosonic fields, $[a_k, a_{k'}^\dagger] = \delta(k-k')$. The dispersion relation $\omega_k = u|k| + vk$ readily provides the group velocity of quantum excitations, such that the classical y and z type solutions here correspond to $k > 0$ and $k < 0$, respectively. For $|v| < u$, the system describes a regular analogue light cone with H having only positive many-body eigenvalues, where v corresponds to a finite tilt of the dispersion relation.

For $|v| > u$ the dispersion relation is overtilted, such that one of the branches (either $k < 0$ or $k > 0$) has now negative energies. Negative energies are meaningful in the following sense. As already pointed out above, the Hamiltonian H here has in principle no more well-defined ground state – indicating a serious instability. However, the eigenvalues remain real, such that the closed quantum system still evolves in a stable fashion. In particular, with a Galilei transformation[2] by, e.g., $-v$, we can undo the tilt (the dispersion relation goes to $u|k|$) and thus return to a regular Hamiltonian with a well-defined ground state. Consequently, for the closed quantum system, there is nothing special about whether or not a particular branch has negative eigenenergies. Matters are markedly different, once we consider open quantum systems. Let us stress though that the Galilei transformation applies to both the system Hamiltonian, as well as to the interaction with the environment. Hence, one cannot change a system from stable to unstable by merely moving with respect to it – thus avoiding what would otherwise be a serious conundrum. However, the inverse may well happen: if we fine tune the parameters of the system such that it implements an overtilted dispersion relation in the laboratory rest frame, the coupling to the environment may indeed be such that the system collapses on very fast time scales (usually given by the typical relaxation rates of the considered quantum hardware).

Returning to spatially varying spacetime metrics, apparent event horizons emerge in this field theory when at a given point v crosses from $|v| < |u|$ to $|v| > |u|$, such that there no longer exist a global transformation to a flat spacetime. Consequently, the system is separated at the horizon into two halves, one with a well-defined ground state (regular or no tilt in the dispersion relation) and one with no ground state (overtilted). In principle, one could now expect already the closed quantum system to be unstable as the two halves could exchange energy (which would thus lead to complex eigenvalues). But as is well known [43], this does not happen for this particular system. Even in the presence of such a horizon, the system is still described by regular, real eigenvalues, such that at least for the closed system, the evolution is still stable (though in general not in a well-defined ground state). The reason for this is that on both sides of the horizon, the above coordinate transformation to (y, z) still applies, such that for these coordinates, there still exist two well-defined branches of the wave solutions moving at different speeds relative to the lab frame. At the horizon, the transition from $|v| < |u|$ to $|v| > |u|$ results in one – but only one – of the two coordinate transformations (either y or z, depending on the sign of v) to be singular. Consequently, the branch without singularity simply moves through the event horizon as if it wasn't there. The other branch (with the singularity) is causally disconnected at the horizon, because wave solutions come to a stand-still. Hence the left and right hand side of this branch do not couple.

[2] Galilei transformations are of course allowed for the here considered simulator systems which operate at velocities far below the speed of light.

Since the system is however not in a ground state, meaningful quantum measurements are best defined by anchoring all observables to a basis with well-defined ground state. This is commonly done [43] by imagining the system to be prepared (in the distant past) in the ground state of a spacetime metric without horizon (e.g., perfectly flat spacetime). When now defining measurements with respect to the new eigenbasis, Hawking radiation emerges. A frequency decomposition of this radiation reveals that it is of thermal nature, given by the surface gravity – e.g., for constant u, the temperature is thus proportional to the energy scale $\partial_x v$, evaluated at the horizon.

Crucially, while for the closed system (or for the actual universe) it therefore seems plausible to have stable spacetime metrics with horizons and a related thermal Hawking radiation, it has to be noted that for simulators coupled to an environment, the above is a highly precarious situation – precisely because of the lack of a well-defined ground state. For instance, while the branch with the singularity may well be exactly separated at the horizon for the closed system, the overtilted part very likely becomes unstable simply due to coupling with the environment (see our above Galilei transformation argument, respectively its inverse). Moreover, it cannot be excluded that a (ever so slightly) nonlocal coupling to an environment effectively couples the two causally separated branches, such that energy can be exchanged across the singularity via environment-assisted tunneling. As we now go on to lattice simulators, stability concerns only pile up.

2.2 Simulation with circuit networks

Here, we summarise our simulation idea by means of quantum circuits, and indicate the main accomplishments of our work.

As we see in Eq. (2), for a system to emulate a field moving on a nontrivial spacetime, we need interactions that provide the terms $\sim \dot{\phi}^2$, $\sim \dot{\phi}\,\partial_x\phi$, and $\sim (\partial_x\phi)^2$. Quantum circuit theory [53, 55, 60, 67] readily provides elements that (in a certain continuum limit) provide such interactions. For a superconducting node j, a finite capacitance (C_j) provides to the Lagrangian $\mathcal{L}$ an energy contribution of the form

$$\mathcal{L} \to \mathcal{L} + \frac{C_j}{2}\left(\frac{\dot{\phi}_j}{2e}\right)^2 , \tag{7}$$

whereas a finite inductance (L_j) between two neighbouring nodes $j+1$ and j provides

$$\mathcal{L} \to \mathcal{L} - \frac{1}{2L_j}\left(\frac{\phi_{j+1}-\phi_j}{2e}\right)^2 . \tag{8}$$

In the continuum limit $\phi_j \to \phi(x)$, we indeed get the terms $\sim \dot{\phi}^2$ and $\sim (\partial_x\phi)^2$, respectively.

However, this alone does not provide a tilt of the dispersion relation. This is where gyrators come into play, see Fig. 1 for a schematic representation and a possible realisation of a mesoscopic quantum gyrator, recently developed in Ref. [72]. As pointed out in Ref. [67], a three-port gyrator, connecting two neighbouring nodes ϕ_{j+1} and ϕ_j to ground (whose phase is set to zero) can be described by the following contribution to the Lagrangian,

$$\mathcal{L} \to \mathcal{L} + G_j(\phi_j\dot{\phi}_{j+1} - \dot{\phi}_j\phi_{j+1}), \tag{9}$$

where G parametrizes the transconductance of the gyrator. Note that the gyrator Lagrangian can be subject to gauge transformations, such that its form is not uniquely determined. In the above chosen symmetric gauge [72], it can be directly related to the transport properties

across the device,

$$2eI_j = \frac{\partial \mathcal{L}}{\partial \phi_j} = G_j \dot{\phi}_{j+1} = 2eG_j V_{j+1}\,, \tag{10}$$

$$2eI_{j+1} = \frac{\partial \mathcal{L}}{\partial \phi_{j+1}} = -G_j \dot{\phi}_j = -2eG_j V_j\,. \tag{11}$$

The gyrator thus has a typical circular transport behaviour, i.e., a voltage at j ($j+1$) induces a current (with reversed sign) at $j+1$ (j). The continuum limit (at least a naive continuum limit, as we discuss in detail below) yields indeed a term of the sought-after form $\sim \dot{\phi}\,\partial_x \phi$ and thus provides a tilt. In fact, it is precisely the above circular transport behaviour, which allows us to develop an illustrative intuitive picture for the physical origin of the tilt. Essentially, the gyrator acts as a "conveyer belt" for plasmon excitations within the chain, transporting signals in opposite directions with different group velocity. Thus it has in essence the same effect as a Galilei transformation (at least in the continuum limit), except that we can in principle control it locally within a given chain by modulating the value of G as a function of j. This anisotropy in the group velocities, is imposed in other proposals for apparent horizons in circuit QED [32, 33, 46] by a time dependent electromagnetic field that sweeps through the circuit. Hence, recreating even a stationary spacetime requires a time dependent circuit, which is not the case when using gyrators. Also, when investigating a non-stationary spacetime such as one with an evaporating horizon which indeed requires a time-dependent flux, using gyrators has the advantage of fixing the position of the horizons in the lab frame and not in the co-moving frame that moves with the sweeping electromagnetic field.

The above ingredient list is in principle sufficient to simulate analogue spacetime geometries with finite curvature. Also, while 1D and 2D arrays are likely most straightforwardly implemented on a circuit board, with appropriate 3D stacking one could potentially also reach a higher number of spatial dimensions. The above realisations mark a first central accomplishment of this work, where

(i) we identify a minimal set of circuit elements to realise scalar discrete field theories with any shape of stationary analogue spacetime geometry.

For illustration purposes and practicality, we stick to 1D arrays in the remainder of this work. However, even in the $1+1$ dimensional problem, there are a number of interesting challenges which we attack in the following. As we argue in more detail below, already for flat spacetime, an overtilt (with a negative energy branch) is not straightforward to realise. As can be seen when comparing Eq. (2) with the inductor contribution of Eq. (8) an overtilt $|v| > u$ requires *negative* inductances. As a second main result (developed in the subsequent section),

(ii) we show how to realise negative inductances via transient flux drive of Josephson junctions, and thus create overtilted dispersion relations and analogue (apparent) event horizons.

This particular implementation of negative inductances via a flux quench is first of all of fundamental interest, as (contrary to other realisations [38, 42]) we do not require a continuous non-equilibrium drive to maintain the event horizons. As we detail further below, the absence of a well-defined ground state is merely the result of an approximation valid at short times. The exact quantum field theory retains a ground state at all times, which will ultimately be reached again via relaxation processes, thus potentially offering the possibility of a complete wormhole evaporation simulation emerging naturally from the hardware. Moreover, the setup we propose allows for a radical change of the spacetime geometry over only a few lattice sites (and as we show in a moment, even over a *single* lattice bond). With the energy scales of the

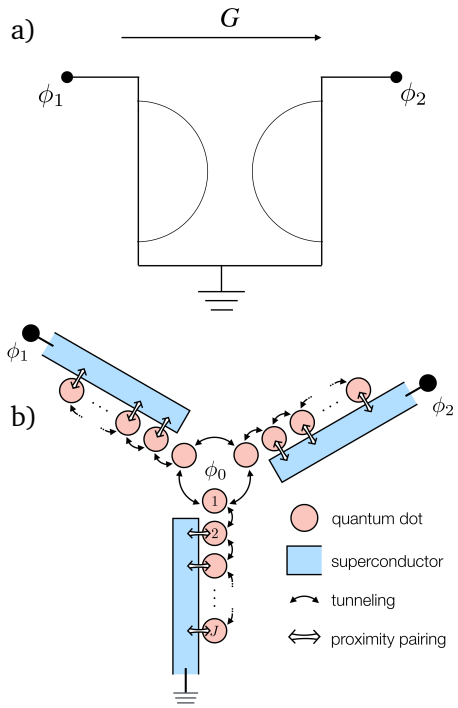

Figure 1: a) Schematic of a gyrator, a four-terminal circuit element, introduced by Tellegen [65]. Here two of its terminals have been grounded, hence it acts as an effective two terminal element. b) One possible realisation of a (quantum) gyrator, as proposed in [72], by using quantum dots proximitized with superconductors. Building up on the prediction of Ref. [73] that conventional multiterminal Josephson junctions harbour topological bands in the space of superconducting phases, one of the goals of Ref. [72] was the development of blueprints to create topological *flat* bands, where the circuit behaviour reduces to Eqs. (10) and (11). The above quantum dot array is one of three proposed ways to generate topological flat bands in multiterminal junctions. Flat bands emerge under appropriate tuning of the central flux (ϕ_0) and for sufficiently long chains (J large). For further details, see Ref. [72].

local charging energy given by E_C and when using Josephson junctions as inductive elements E_J, we would thus (at least in principle) be able to reach Hawking temperatures (as defined above) on the order of $\sim \sqrt{E_C E_J}$ which (taking as a typical transmon qubit frequency the value of 1GHz $\sim$ 10GHz) can yield up to 0.1K $\sim$ 1K (which is above typical cryogenic temperatures).

However, in addition to the already mentioned general stability issues related to the environment, the circuit simulation reveals fundamental lattice-specific spontaneous instabilities (due to complex eigenvalues), which are already present when disregarding the environment. We expect those to impede a straightforward observation of thermal Hawking radiation. Instead,

(iii) we propose to directly probe the spontaneous collapse of systems with apparent event horizons by means of accumulating quantum fluctuations, which we argue to be distinguishable from collapse due to dissipative processes.

At any rate, some of the lattice-specific stability issues can be appreciated on the general level here, others will be shown subsequently for a specific model. On a general footing, we see in Eq. (2) that any (constant or spatially dependent) local tilt v (which in our simulation would be implemented by constant or spatially varying gyrator parameters G_j) must equally appear in the $(\partial_x \phi)^2$ term, as the corresponding matrix element g^{11} ($\mu, \nu = 1$ is the space-space

component) is proportional to $v^2 - u^2$. In other words, a finite nonreciprocity in the circuit needs to be "countered" by a corresponding inductive interaction, in order to realise actions of the form of Eq. (2). Consequently, we would need an according spatially dependent tuning of the local inductance profile L_j which matches exactly with the values of G_j. But first of all, such a perfect fine tuning is realistically not possible, such that the condition $g = -1$ is in general only approximately, but never exactly, fulfilled. Hence, the mapping onto Eq. (5) is likewise not exact, and we cannot guarantee a perfect causal decoupling across the horizon, and the closed system might become spontaneously unstable over already short time scales. In fact, below we refrain from a simulation with constant metric determinant g (in fact, we will modify the inductances rather than the gyrator values), such that the systems we consider do not map to Eq. (5) in the continuum limit. Furthermore, with the Hawking temperature being defined (at least in continuous field theories) as the derivative of the group velocity (i.e., the surface gravity) at the event horizon, there emerges the curious question of what happens to the observables of the system when considering a very sharp (discontinuous) change of the metric at the horizon, and how such a diverging surface gravity is regularized. In what follows we will provide an answer to that question for lattice simulators. It should be noted that step like horizons have been studied in continuum approximation in the context of BECs [125,126]. In these works, unlike ours, scattering modes with real eigenenergies form a complete basis. Therefore, it is still possible to define a scattering mode where an incoming negative norm mode scatters to an outgoing positive norm mode. This mode is often termed the "Hawking mode", and its flux can be used to deduce the spectrum of the Hawking radiation.

Moreover, there is a deeper issue that our discrete circuit realisation unravels, which is true even if perfect tuning of G_j and L_j would be available. To see this, consider first an (infinite) array where all gyrators have the same parameter $G_j = G$. Here, we can reformulate the nonreciprocal part of the Lagrangian as follows,

$$G\sum_j \left(\phi_j\dot{\phi}_{j+1} - \phi_{j+1}\dot{\phi}_j\right) = G\sum_j \dot{\phi}_j\left(\phi_{j-1} - \phi_{j+1}\right). \tag{12}$$

Thus, we see that in order to have the correct counter term in the g^{11} component for the lattice, we actually do *not* need nearest neighbour inductive coupling [as indicated in Eq. (8)] but instead *next-to-nearest* neighbour coupling, $\sim(\phi_{j+1} - \phi_{j-1})^2$. As further detailed below, because of this fundamental feature of the gyrator element, nearest and next-to-nearest neighbour inductive couplings have fundamentally different stability properties. In particular,

(iv) we find an important loop hole to the ambiguous black and white-hole nature of lattice event horizons (through an EP in the dispersion relation) leading to a fundamentally different behaviour in the wormhole interior.

Finally, when returning to a spatially varying G_j, we can draw another important conclusion. Namely, for a general gyrator Lagrangian of the form

$$\sum_j G_j\left(\phi_j\dot{\phi}_{j+1} - \phi_{j+1}\dot{\phi}_j\right) = \sum_j \dot{\phi}_j\left(G_{j-1}\phi_{j-1} - G_j\phi_{j+1}\right), \tag{13}$$

it turns out to be impossible to find exact inductive counter terms: as can be seen in the right-hand side of above equation, the Lagrangian can no longer be factored into simple phase differences (due to $G_j \neq G_{j-1}$). The only possibility to counter the above expression in terms of inductive couplings is to add inductors to ground, and thus abandon charge conservation within the array. While charge leakage to ground is very much a potential reality (especially if the realisation of the gyrators is not ideal, leading to additional inductive shunts), nonetheless

(v) we conclude that for generic circuits networks, nonreciprocal interactions cannot be exactly countered by charge conserving inductive interactions.

The breaking of charge conservation (which is physical as it corresponds to leakage to ground) effectively provides a mass term in the theory. In fact, we will include a (finite but very small) mass term in the following, but for a different reason: it allows us to deal with the otherwise problematic zero mode in the boson Hamiltonian.

To summarise, items (i) and (v) have already been fully demonstrated within the above general reasoning, and require no further illustration. Items (ii-iv) on the other hand are now explicitly shown in what follows, by considering a concrete setup.

3 Setup

We here show with two example circuit models the capability of circuit arrays to engineer nontrivial dispersion relations with analogue wormholes. The first proposed circuit consists of an array of J nodes (with periodic boundary conditions, i.e., $J+1=1$), interconnected via Josephson junctions in parallel with 3-port gyrators, as depicted in Fig. 2a). The complete Lagrangian of the circuit will consist of three parts, namely a capacitive Lagrangian in Eq. (7), a gyrator Lagrangian in Eq. (9) and a term for the Josephson junctions $\mathcal{L}_J = \sum_{j=1}^{J} E_J \cos\left(\phi_{j+1} - \phi_j + \phi_{\text{ext},j}\right)$. Here, E_J is the Josephson energy and $\phi_{\text{ext},j}$ is the external flux coupling to each Josephson junction. This flux, and its time-dependent control, will play a pivotal role in what follows.

The Lagrangian of this circuit can be written as

$$\mathcal{L} = \sum_{j=1}^{J} \left[\frac{C}{2} \left(\frac{\dot{\phi}_j}{2e} \right)^2 + G\phi_j \left(\dot{\phi}_{j+1} - \dot{\phi}_{j-1} \right) + E_J \cos\left(\phi_{j+1} - \phi_j + \phi_{\text{ext},j} \right) \right] . \tag{14}$$

To get to the Hamiltonian we first define the conjugate variable $N_j = \partial \mathcal{L} / \partial \dot{\phi}_j$ and then perform the Legendre transform $\mathcal{H} = \sum_j \dot{\phi}_j N_j - \mathcal{L}$, in alignment with standard circuit quantisation [53, 55]. We find that the Hamiltonian of this array takes the form

$$\mathcal{H} = \sum_{j=1}^{J} \left[E_{\text{C}} \left[N_j + G(\phi_{j+1} - \phi_{j-1}) \right]^2 - E_J \cos(\phi_{j+1} - \phi_j + \phi_{\text{ext},j}) \right] , \tag{15}$$

with the charging energy

$$E_{\text{C}} \equiv \frac{(2e)^2}{2C} .$$

The number operator N_j and the phase ϕ_j satisfy the canonical commutator $\left[N_j, \phi_{j'} \right] = i\delta_{jj'}$.

As stated in the previous section, the stability of circuits where Josephson junctions connect nearest neighbours nodes and the ones where Josephson junctions couple next nearest neighbour nodes is very different. Therefore, to illustrate their differences the second circuit we study has next nearest neighbour connections via Josephson junctions, see Fig. 2b). The Hamiltonian for such a circuit is

$$\mathcal{H}' = \sum_{j=1}^{J} \left[E_{\text{C}} \left[N_j + G(\phi_{j+1} - \phi_{j-1}) \right]^2 - E'_J \cos(\phi_{j+1} - \phi_{j-1} + \phi_{\text{ext},j}) \right] . \tag{16}$$

Considering the system at low energies (close to the many-body ground state), the phases on the nodes will approach an equilibrium configuration minimizing the total Josephson junction energy of the array. For sufficiently long arrays, we find either $\phi_{j+1} - \phi_j \approx -\phi_{\text{ext},j} + \delta\phi_{j+1} - \delta\phi_j$ (for $\mathcal{H}$) or $\phi_{j+1} - \phi_{j-1} \approx -\phi_{\text{ext},j} + \delta\phi_{j+1} - \delta\phi_{j-1}$ (for $\mathcal{H}'$). Assuming $E_C < E_J$, the quantum fluctuations around the equilibrium value will be small,

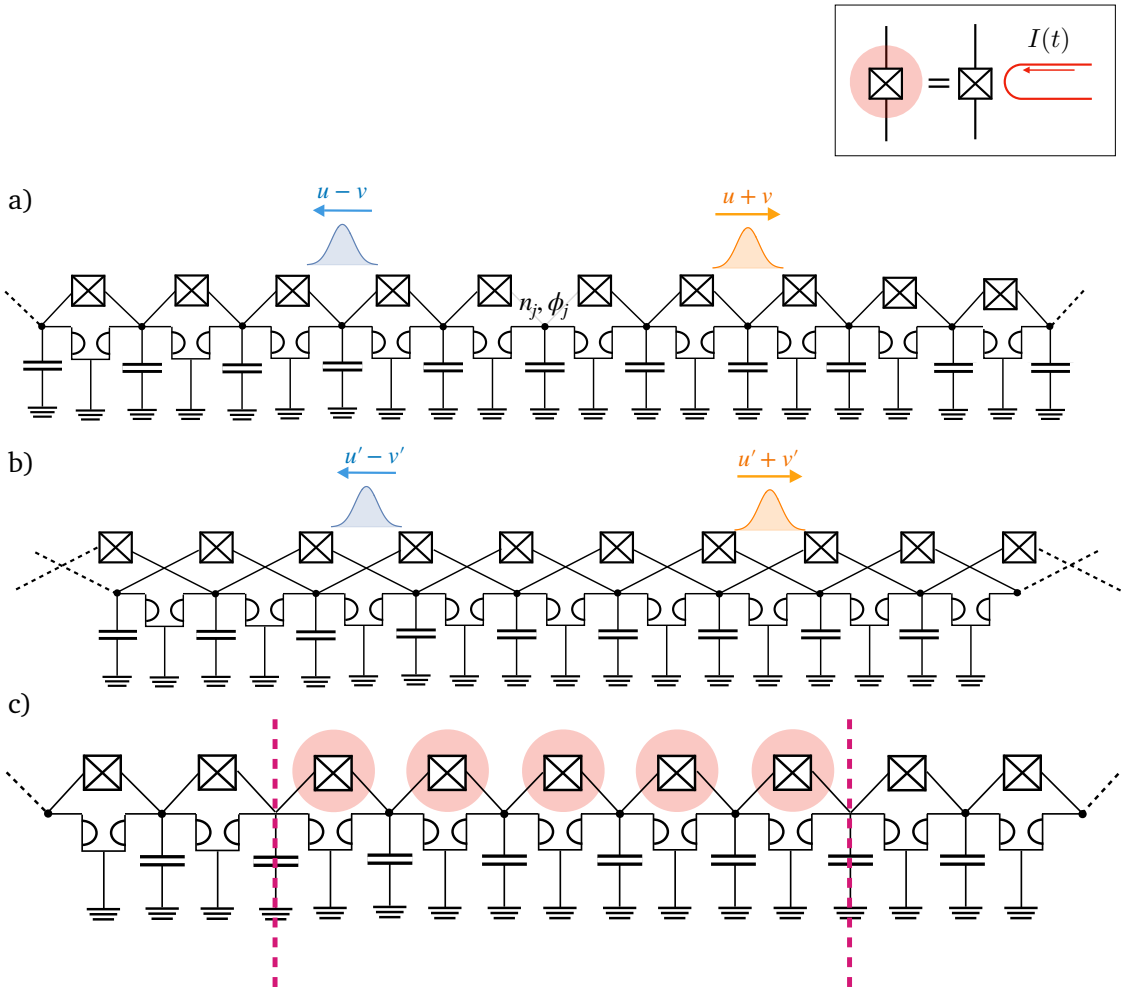

Figure 2: Wormhole simulations with quantum circuits. In circuits a) and b) (nearest and next-to-nearest Josephson coupling, respectively) the presence of gyrators tilts the dispersion relation giving left and right moving wave packets different speeds. The circuit c) is obtained by inverting the signs of a finite connected region inductances of circuit a). This is achieved by a flux quench induced by a localised current (inset), shifting the superconducting phase difference across the junction by π, leading to negative inductance. This creates two boundaries between the normal and over-tilted regions, which act as the apparent horizons. Horizons for the circuit with Josephson junctions connecting next-nearest neighbours b) can be obtained in a similar manner.

$\delta\phi_j \ll 1$. Consequently, the Josephson term in Hamiltonians (15) and (16) can be approximated by

$$\begin{aligned} &\approx \sum_{j=1}^{J} E_L(\delta\phi_{j+1} - \delta\phi_j)^2 + \text{const.} \\ &\approx \sum_{j=1}^{J} E'_L(\delta\phi_{j+1} - \delta\phi_{j-1})^2 + \text{const.}, \end{aligned} \tag{17}$$

where $\delta\phi_j$ still satisfy the same commutation relations with N_j. The inductive energy is $E_L^{(\prime)} = E_J^{(\prime)}/2$.

With the quadratic approximation of the Josephson energies,[3] the total Hamiltonian describes a noninteracting boson field. Moreover, close to the ground state, the externally applied flux $\phi_{\text{ext},j}$ could be eliminated from the problem. It would therefore seem that neither the non-linearity of the Josephson junction, nor the external flux play a role. However, as we will show in Sec. 4, transient flux-control and the compact cosine behaviour of the Josephson energy will allow us to generate nontrivial features related to quantum gravity. In particular, we will be able to modulate the effective inductive energy E_L highly locally, and in particular, render it negative, allowing for the creation of instabilities that will lead to non-thermal Hawking radiation. Note that the non-linearity of the Josephson energy was likewise of importance for earlier proposals to measure Hawking-like radiation emerging from soliton excitations in Josephson junction arrays [33]. We will comment on similarities with – but also significant differences to – our approach further below.

For the above conventional non-interacting boson problem, translational invariance allows us to analytically diagonalise the Hamiltonians (15) and (16), $\mathcal{H}^{(\prime)} = \sum_m \omega_m^{(\prime)} b_m^\dagger b_m$ (where index m goes from $-J/2+1$ to $J/2$), to get the dispersion relations (Appendix A)

$$\begin{aligned} \omega_m &= 2\sqrt{E_C^2\beta_m} + 4E_C G \sin\left(\frac{2\pi m}{J}\right), \\ \omega'_m &= 2\sqrt{E_C^2\beta'_m} + 4E_C G \sin\left(\frac{2\pi m}{J}\right), \end{aligned} \tag{18}$$

where b_m ($b_m^\dagger$) are bosonic annihilation (creation) operators satifying $[b_m, b_{m'}^\dagger] = \delta_{mm'}$ and

$$\begin{aligned} \beta_m &= \frac{4E_C G^2 \sin^2\left(\frac{2\pi m}{J}\right) + 4E_L \sin^2\left(\frac{\pi m}{J}\right) + M}{E_C}, \\ \beta'_m &= \frac{4E_C G^2 \sin^2\left(\frac{2\pi m}{J}\right) + 4E'_L \sin^2\left(\frac{2\pi m}{J}\right) + M}{E_C}, \end{aligned} \tag{19}$$

where we will set $E'_L = E_L/4$ for the ease of comparing the two spectra in the linear approximation. The quantum number m enumerates the momentum of bosonic excitations, where we can define the wave vector as $k = 2\pi m/J$, such that $\omega_m^{(\prime)} \to \omega^{(\prime)}(k)$. Note that we have introduced a very small mass term M ($\mathcal{H}^{(\prime)} \to \mathcal{H}^{(\prime)} + M\sum_j \phi_j^2$) to avoid the well-known diagonalisation issues with the zero modes. We take whenever possible the limit $M \to 0$. The mass term physically corresponds to a small leakage of supercurrent towards ground, which could, e.g., originate from an imperfect implementation of the gyrator element.

[3] For high Josephson energies, breaking compactness of the phase variable is unproblematic, at least in the present case. In the opposite regime of weak Josephson energies we cannot ignore the fact that superconducting phases live on a compact manifold, i.e. $\phi_j \in \{0, 2\pi\}$. One peculiar consequence of compact phases is that the allowed values of the gyrator conductance G have to be quantised (as per Dirac's monopole quantisation), which provides an entirely different behaviour of the superconducting chain such as anyonic excitations [72].

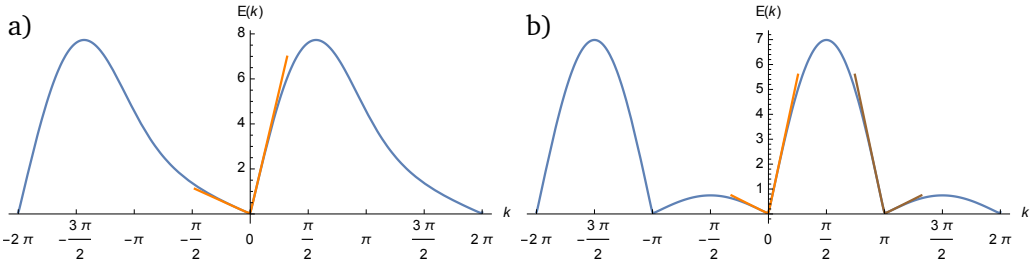

Figure 3: The above two figures show that the low-momentum eigenvalues (blue lines) of the circuit Hamiltonians (15) and (16) can be approximated by the linear dispersion relation (20) (orange lines) at low energies. The branches of the dispersion relation correspond to right and left movers with speeds $u \pm v$. One crucial point about the eigenvalues in b) is that near $k = \pi$ the dispersion relation (brown lines) is the mirror image of the dispersion near $k = 0$, which is a feature that the eigenvalues in a) do not have. Parameters used: $E_C/E_L = 1.3, E_L'/E_L = 0.25, G = 0.6$, and $J = 50$. To lift the degeneracy at zero energy, a small mass term is used ($\approx 10^{-3} E_L$).

For small k, the system exhibits a linear dispersion relation, [see Figs. 3a) and 3b)],

$$\omega(k) \approx \omega'(k) \approx 2\sqrt{4E_C^2 G^2 + E_C E_L}\,|k| + 4E_C G k\,. \tag{20}$$

In the relativistic sense, this would correspond to the analogue speed of light, where the two branches $k > 0$ and $k < 0$ denote right and left moving signals, respectively [see also Eq. (6)]. Importantly, we see in general different analogue speeds of light $u + v$ ($u - v$) for excitations moving to the left, $k < 0$ (right, $k > 0$) [as illustrated in Figure 2a) and 2b)], with $u \propto 2\sqrt{4E_C^2 G^2 + E_C E_L}$ and $v \propto 4E_C G$. A nonzero v corresponds to a tilt of the dispersion relation, which is only possible for a nonzero gyrator, $G \neq 0$, due to the aforementioned "conveyer belt" dynamics.

Moreover, we observe that on this coarse-grained level (small k essentially corresponds to taking the continuum limit of the lattice grid), the two models exhibit the exact same dispersion relation. Note however, that the next-nearest neighbour model hosts a second low-energy point with linear dispersion relation at $k \approx \pi$ [see Fig. 3b)], in accordance with Ref. [48]. The dispersion tilt here is always opposite to the one at $k \approx 0$. This feature emerges for the following reason. In the absence of the gyrators, the model $\mathcal{H}'$ has two disjoint low-energy fields for even and odd lattice sites, resulting in a π-periodic Brillouin zone. The gyrators couple these two separate modes, restoring 2π-periodicity with respect to k (due to the alternating tilt), but keeping the two low-energy solutions intact. In essence, while model $\mathcal{H}$ hosts a single low-energy analogue light field, model $\mathcal{H}'$ hosts two separate fields with opposite dispersion relation. This detail will play an even more prominent role in what follows.

In order to engineer analogue wormholes with event horizons, we need to specifically create a dispersion relation with an *overtilt* where $|v| > u$ – at least in a finite region of the device. Therefore, the central object to consider is our resulting dispersion relation, Eq. (20). Dividing the frequency by the reference energy E_C we are left with only two dimensionless quantities, G and E_L/E_C. While $|E_L/E_C|$ must be greater than unity to justify the quadratic approximation, G can, in principle, be both larger or smaller than unity (see footnote 3 for restrictions on values of G due to phase compactness). At any rate, the relative magnitude of G versus E_L/E_C has little bearing on the observed phenomenology. However, the goal of creating an overtilt provides us with a significant challenge: if both the inductive and capacitive energies E_L, E_C are positive, then it can be easily shown that $u > |v|$, independent of the specific parameter values. Consequently, an overtilt must necessarily involve negative capacitances or negative inductances. In the next section, we will explicitly discuss possibilities to render

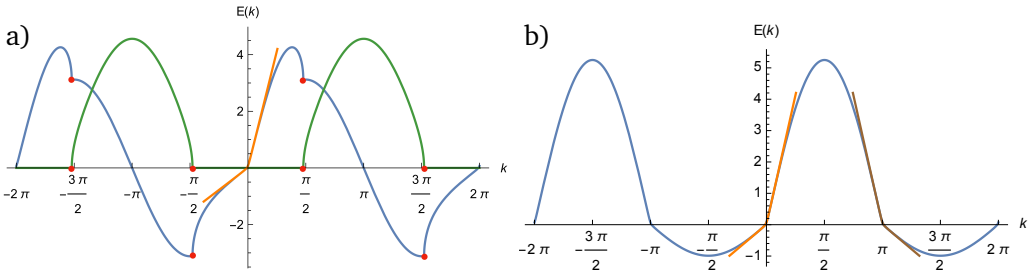

Figure 4: The principle behind the topological loop-hole for black versus white hole horizons in lattice systems via EPs. In panels a) and b), we show the complete dispersion of the circuit Hamiltonians (15) and (16) with negative inductances. When the Josephson junctions connect nearest neighbours, a), the eigenspectrum is complex (blue line represents real part of the eigenvalues and the green line the imaginary part). The points where the eigenvalues go from real to complex are EPs (marked by red dots). Consequently, the spectrum only crosses zero once at $k = 0$, and satisfies the periodicity constraint of the Brillouin zone via a detour in the complex plane. For next nearest neighbour coupling, b), the spectrum is real for all values of k, and crosses zero twice, again with mirror images at $k = 0$ and $k = \pi$. The low momentum eigenvalues (orange line) for both the circuits do show an overtilt, which is required to create a horizon. Parameters are same as in Fig. 3, except the signs for E_L and E_L' are flipped.

either E_C or E_L negative, and point out in particular, why we expect negative E_L to be the more feasible of the two options.

In the remainder of this section, we proceed by discussing the consequences a negative inductance has on the dispersion relation. As already stated, for small k we thus get an overtilted linear dispersion relation in both models, see Figs. 4a) and 4b). As the slope of the dispersion relation now has the same sign for both positive and negative k, we get signals propagating in the same direction. If we now join regions with regular ($u > |v|$) and overtilted ($u < |v|$) dispersion relation, we could indeed engineer analogue wormholes. But before we embark on that, we need to discuss in detail the behaviour of the dispersion relations, Eq. (18), for large k. Namely, when considering the full Brillouin zone (i.e., for $-\pi < k < \pi$), we see that the two models (nearest versus next-nearest neighbour) differ significantly. In particular, for the nearest neighbour coupling, we observe that outside the range $-k_0 < k < k_0$ the dispersion relation becomes complex, see Fig. 4a), where k_0 is determined by the condition

$$\sin^2\left(\frac{k_0}{2}\right) = \frac{4E_C G^2 - |E_L|}{4E_C G^2}\,. \tag{21}$$

This transition point is equivalent to an *EP* in the system. Crucially, this finding is in stark contrast to the model circuit where the Josephson junctions connect the next nearest neighbours. Here, for parameter regime $4E_C G^2 + E_L > 0$, we can overtilt the dispersion relation without encountering complex eigenvalues, see Fig. 4b).

Before moving ahead we would like to address the seeming incongruity of having complex eigenvalues for a Hermitian Hamiltonian, as we just observed in the case of nearest neighbour coupling with negative inductance. We did preempt this in Sec. 2.1, by stating that existence of complex eigenvalues implies instability in the system. But still this result might be confusing as the Hamiltonian we are working with remains Hermitian at all times, in short this problem comes around because we are being cavalier with the word “eigenvalues”. Looking at Appendices A and B, one can see that to diagonalise the Hamiltonian we have to eventually perform

a bosonic Bogoliubov transformation. It is a well known fact that for bosons the Bogoliubov transformation involves finding eigenvalues of a non-Hermitian matrix. If these eigenvalues are real then one can go ahead and diagonalise the original second quantised Hamiltonian, and realise that the eigenvalues of the second quantised Hamiltonian correspond to the eigenvalues of the non-Hermitian matrix. On the other hand, if the eigenvalues of the non-Hermitian matrix are complex, the idea that Bogoliubov transformation is diagonalising the second quantised Hamiltonian goes out the window [122]. Instead, the Bogoliubov transformation brings the Hamiltonian in the following form: $\mathcal{H} = \sum_i \lambda_i b_i' b_i$. Here, the operators b_i' and b_i follow the CCR but are not related to each other via Hermitian conjugation, and λ_i, which are the eigenvalues of the non-Hermitian matrix, are complex. Still, this kind of Bogoliubov transformation is useful, as it makes studying the dynamics of the system much easier, which is what we do in Sec. 5. A more thorough exploration of under what conditions a quadratic bosonic Hamiltonian is diagonalisable using Bogoliubov transformation can be found in [127].

There are several reasons why both of these models are interesting in their own right. First, let us comment in more detail on stability. In principle, the inversion of inductance (or capacitance for that matter) indicates a spontaneous electrostatic instability. This can be understood already on a much simpler level of a single LC circuit, with a resonance frequency $\sim \sqrt{E_L E_C}$. Swapping the sign of the inductance leads to an imaginary frequency. Note that for transient times, this result is by no means problematic (see also Sec. 2.1), as such an imaginary frequency corresponds to placing a localised wave function on the tip of an inverted harmonic potential. For transient times, we can by all means obtain physically meaningful results from the Schrödinger equation. In particular, note that such an evolution will result in an exponential blowing up of quantum fluctuations of both canonically conjugate quantities, here, charge and phase (as we will see later also in explicit calculations). This might at first sight seem counterintuitive. The most common situation for generic quantum wave functions is that the uncertainty in one of the two conjugate spaces is inversely proportional to the uncertainty in the other. But note that inverted potentials provide very special wave functions over time that spread both in position (e.g., ϕ) space, as the wave function evolves from the tip of the parabola to both sides, as well as increasing uncertainty in momentum (e.g., N) space, since the particle wave gets more and more accelerated as it rolls down both sides of the inverted parabola. The theory is only problematic in the long-time limit, due to the formal removal of a well-defined ground state. We note that our realisation of negative inductances via the inherent non-linearity of the Josephson effect provides a very neat conceptual realisation of instabilities, while (in principle) retaining a well-defined ground state for long times, as we explain in more detail further below. We also note that a recent work [128] has explored a related but distinct concept of negative mass resonators in cQED architectures, by strongly driving a weakly nonlinear superconducting LC circuit [129], leading effectively to negative susceptibility.

To proceed, we note that in the 1D chain models we consider, there are ways to stabilise the system in spite of negative inductances, in line with the discussion in Sec. 2. Indeed, the gyrators play the pivotal role for stabilisation: in the Hamiltonians of Eqs. (15) and (16), when we expand the term in the first line $\sim E_C$, we get an effective inductive element due to a nonzero G, $\sim E_C G^2(\phi_{j+1} - \phi_{j-1})^2$. This is an effective inductive contribution due to the gyrator, which is guaranteed to be positive even when $E_L < 0$ (as long as $E_C > 0$). But as already foreshadowed in Sec. 2.2, this effective inductive contribution couples next-nearest neighbour sites. Hence, a negative next-nearest inductor [Eq. (15)] can be exactly compensated by a positive next-nearest neighbour contribution of the gyrator. The negative nearest neighbour inductor model [Eq. (16)] on the other hand cannot exactly be compensated by the gyrators, hence the presence of the EP.

Let us now take a bit of a more formal perspective on the above observation for generic wormhole simulations, which will allow us to demonstrate one of the central results of this work, see also item (iv) in Sec. 2.2. Namely, there is a simple topological connection between overtilted spectra, Brillouin zone sizes, and EPs. For discrete lattice implementations the dispersion relation is always 2π periodic in k. Crucially, an overtilted spectrum means that the energies cross from positive to negative values at the transition points $k = 0, 2\pi, \ldots$. If the spectrum is real for all k, then periodicity in momentum space always guarantees that an overtilted spectrum near a certain value of k must have an overtilted partner at another value of k with *opposite tilt direction*, as a periodic spectrum must traverse the zero-energy line an even number of times (essentially a simplified version of the Nielsen-Ninomiya theorem [48]). Consequently, for any lattice implementation, it seems unavoidable that what appears like a black hole horizon near one value of k, must necessarily have a white hole horizon partner at another value of k. This fact has already been pointed out in the context of analogue black-hole simulations in tilted Weyl semimetal structures [31, 130]. Our next-nearest neighbour model confirms this expectation, where the overtilt point at $k \approx 0$ has an inverted partner point at $k \approx \pm\pi$, see Fig. 4 b). These two k points can be individually addressed when preparing, e.g., Gaussian wave packets centered either around $k \approx 0$ (wave packets that are smooth in j space) and $k \approx \pm\pi$ (wave packets with alternating even-odd signs in j space).

Crucially, the nearest-neighbour model provides an intriguing conceptual loop hole: here, the overtilt at $k \approx 0$ has no partner point with inverted tilt, very simply because the dispersion relation satisfies the periodicity constraint in k by taking, in a sense, a "detour" in the complex plane – by courtesy of the EP. Consequently, the spectrum crosses the zero energy line only once. We are thus able to conclude that there is after all a case, where black and white hole horizons can be created independently in a lattice. This comes at the cost of a spontaneous instability within the overtilted region, which, importantly, is present even in the absence of an event horizon. This finding will be of great importance when interpreting the origin of radiation in the presence of event horizons in Sec. 5 below.

4 Realising negative inductance through quench

As noted above, an overtilt in the dispersion relation is realised by means of either negative capacitances or negative inductances. We here present ideas for the engineering of both features, and then argue, why we expect the latter to be more feasible, thus demonstrating claim (ii) in Sec. 2.2,

Negative (and other nonlinear) capacitances are an interesting topic within quantum circuits, which date back to various pioneering ideas by Little [131] and Landauer [132], and have recently been a focal point of research, either in the form of ferroelectric materials [133–136], or capacitively-coupled polarisers inducing pairing in quantum dots [137, 138]. Specifically within the circuit QED context, it has recently been proposed that negative capacitances exist in the sense of an emf-induced renormalisation [60], or that the charge in the quantum phase slip energy contribution can be fractionalised and thus rendered incommensurate [139, 140]. There is, however, the problem that negative capacitances correspond to an electrostatic instability, and are thus only meaningful either as partial capacitances (where another capacitance in parallel guarantees total positivity on a given charge island) or in a transient regime. Since we are interested in the latter (after all, Hawking radiation is manifestly a transient feature), this means that the capacitance would have to be tunable on very fast time scales, which seems challenging, especially on the small scales of the here proposed circuit QED architecture.

This is why we move on to ideas on how to bring about a transient behaviour within the inductive (Josephson junction) element. Remember that we focus on a regime of $E_J > E_C$

where the cosine of the Josephson energy can be approximated as a parabola with the inductive energy $E_L \sim E_J$ of an effectively regular linear inductor (rendering the resulting plasmon field effectively non-interacting, as shown above). Nonetheless, we can exploit the nonlinear inductive behaviour. Suppose there is a mechanism, allowing for a fast, transient switch from $-\cos(\phi_j - \phi_{j-1})$ (e.g., for the nearest neighbour model) to $+\cos(\phi_j - \phi_{j-1})$. If that switch occurs sufficiently fast, the circuit degrees of freedom have no time to adjust, such that the many-body wave function immediately after the switch remains localised on what is now the *maximum* (and not the minimum) of the cosine. Expanding for small phase differences localised around said maximum, we can realise a sign switch of the inductive energy, $E_L \to -E_L$, leading to the sought-after overtilt in the dispersion relation (see the orange lines in Fig. 3). Specifically, in the next section, we discuss the possibility of applying an inverted inductance only in part of the system to create event horizons separating regions with $u < |v|$ from unquenched regions with $u > |v|$.

Our proposal, thus, requires a mechanism to locally address the Josephson junctions in a way to create connected regions with inverted inductance. We note that so-called tunable $0-\pi$ junctions are a subject of ongoing research and have multiple proposals for their implementation, including the theoretical proposal about Josephson junctions with a high-spin magnetic impurity sandwiched between two superconductors [100], experimental realisation in ballistic Dirac semimetal Josephson junctions [101] and another experimental realisation in Indium antimonide (InSb) two dimensional electron gases [102].

We here point out a feasible alternative, where inductance inversion is also possible for regular superconductor-insulator-superconductor Josephson junctions. Namely, a nearby current source can likewise induce a phase shift of π. This idea is based on the results of Ref. [60] where a gauge invariant formulation of time-dependent flux driving was derived. Gauge aspects are of utmost importance to understand how time-dependent flux is allocated in circuits involving multiple Josephson junctions, such as SQUIDs or junction arrays [60, 99, 141]. Previous to Ref. [60], it was expected that the ordinary lumped element approach to circuit QED is valid in the presence of time-dependent flux. In this standard framework, it was recently shown [99] that the allocation of the time-dependent flux within the device (and thus, of the induced electric fields) is given by the capacitive network of the involved charge islands. If this observation were generally true, it would be difficult to locally address certain junctions with high local precision, unless the capacitive network would be engineered accordingly. However, as shown in Ref. [60], the connection between flux allocation and the capacitive network is valid only in special cases; in general, both device geometry and magnetic field distribution lead to a highly nontrivial flux allocation.

We here adopt this principle to show that the individual junctions can be addressed by small current loops, (one loop per junction) where a time-dependent drive (inset in Fig. 2) provides a shift inside the Josephson energies of the form $\cos(\phi_{j+1} - \phi_j + \phi_j^{\mathrm{ext}})$, where

$$\phi_j^{\mathrm{ext}} = \frac{2\pi}{\Phi_0} \int_{\mathcal{L}_j} d\mathbf{l} \cdot \mathbf{A}. \tag{22}$$

Here Φ_0 is the flux quantum and $\mathbf{A}$ is the vector potential in the irrotational gauge [60, 99] accounting for the magnetic field emitted by the current carrying loop sources. Note that since the magnetic field decays only as a power law, one may have to take into account non-local effects, that is, the current loop at junction j influences not only the phase drop at junction j but also at the other junctions j', see Fig. 5a). We can generically write down the equation

$$\phi_j^{\mathrm{ext}}(t) = \sum_{j=1}^{J} \alpha_{j,j'} I_j(t), \tag{23}$$

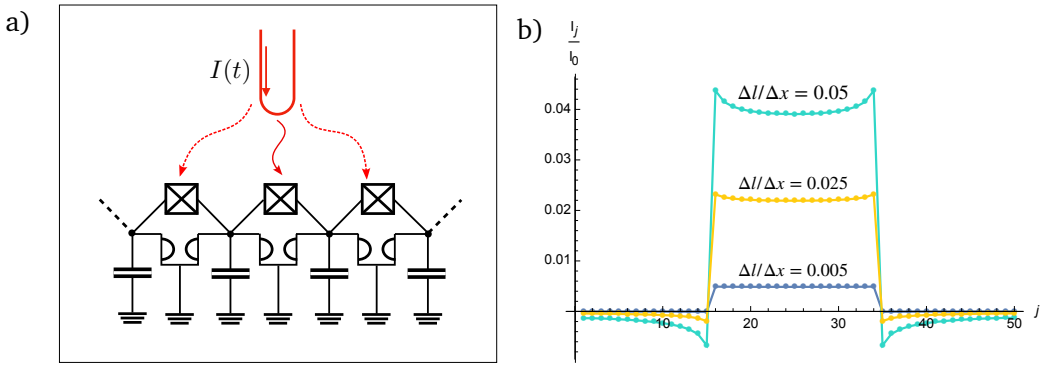

Figure 5: Illustration of non-local effects of the current loop flux drive. In order to create the target phase shift profile of exactly π within a connected region in the junction array (from $j = j_0$ to $j = j_1$), the corresponding applied current profile as a function of site index j needs to be slightly nonlocal. We have plotted three current profiles, that were obtained for a system with 50 sites with $j_0 = 15$ and $j_1 = 35$, with different ratios of Δl to Δx as shown in the graph. The parameter R does not have a significant effect on the nature of the current profile, only on the magnitude of the ratio I_j/I_0, hence we set $R/\Delta x = 1$.

where the matrix α contains the information about the geometric details of the circuit, and accounts for the screening of the magnetic field (Meissner effect) as well as the screening of the induced electric field (Thomas-Fermi screening). In order to know what exact current pulses need to be applied in order to create a desired target phase profile ϕ_j^{ext} (e.g., $\phi_j^{\text{ext}} = \pi$ within a given connected interval, $j_0 < j < j_1$, and $\phi_j^{\text{ext}} = 0$ everywhere else, which gives the black and white hole horizons, see sections below), one simply needs to invert the square matrix α. Generally, we note that for our purposes, the precision requirements are not so stringent: as long as deviations from the target phase profile are small (with respect to π), the inductances in the array are still inverted, resulting in the desired apparent event horizon.

The computation of matrix α is in general a complicated numerical task. We can however provide a rough estimate by assuming the junctions to be arranged in a straight line, and applying the Biot-Savart law (similar in spirit to Ref. [142]). To this end, we assume that each current-carrying wire j is described by a small current element of length ΔL. For small current loops with radius R, we can simply set $\Delta L \sim R$.[4] Assuming Coulomb gauge (equivalent to the irrotational gauge, up to screening of induced charges on the superconducting surfaces [60], which we here neglect for simplicity) we have to solve $\nabla^2 \mathbf{A} = -\mu_0 \mathbf{j}$ with the current density $\mathbf{j}$ for a small current carrying element. Assuming an infinitesimal, delta-like current element $\mathbf{j} \sim \delta(\mathbf{x})\mathrm{x}$, and plugging the resulting $\mathbf{A}$ into Eq. (23), we find

$$\alpha_{j,j'} \approx \frac{1}{I_0} \frac{R}{\sqrt{\Delta x^2 (j-j')^2 + \Delta l^2}}, \tag{24}$$

where Δx is the separation between Josephson junctions, and Δl is the separation between current loop j and junction j. The characteristic current I_0 is given as $I_0^{-1} = \mu_0 \mathcal{L}/(2\Phi_0)$, where $\mathcal{L}$ is the length of path $\mathcal{L}_j$ in Eq. (23). It represents the size of the fine structure containing the Josephson junction (Niemayer-Dolan bridge). For a typical size of $\mathcal{L} \sim 10\mu m$, we find $I_0 \sim 10\mu A$ (which is at the upper bound of the current that can usually pass through flux lines). Note that this is a crude upper bound for I_0. Very likely, I_0 is reduced significantly

[4] Note that the most common designs for flux control, the loops have a radius larger than the separation of the input and output lines, such that the representation of the source as a small current carrying element is strongly simplified. A current source with ring geometry could be more precise, but complicates the here presented estimate.

due to screening of the electric field which has here been neglected. We therefore expect that a flip of the phase by $\sim \pi$ is feasible. The other central figure of merit is the speed with which the phase flip can be performed. Defining the ramping time from zero current to target current for a single flux line as Δt_I, the phase flip is guaranteed to be nonadiabatic for $\sqrt{E_C E_J}\Delta t_I < 1$. This requires either the use of sub-GHz qubit designs, similar in spirit to a recent proposal in Ref. [68], or ultrafast ($\sim$ 100 gigasamples per second) arbitrary waveform generators. The latter may cause problems with usual Al-based architecture, but improvements were very recently demonstrated in connection with Nb-based circuits [143].

For the matrix given in Eq. (24), we can explicitly compute a required current profile that needs to be applied in order to swap the phases by $\pm\pi$ within a connected part of the 1D chain. Blue dots in Fig. 5 show that if $\Delta l \ll \Delta x$, α is almost perfectly diagonal, such that there is a one-to-one correspondence between the desired target phase profile and the required current profile that has to be applied to the individual loops. Note however that the onset of non-local effects may play a role even for (moderately) small $\Delta l/\Delta x$ (orange and brown dots in Fig. 5), where we need to apply a slightly nonlocal current profile to have a sharp, local switch from positive to negative inductances within the 1D chain.

Alternatively, $\pm\pi$ shifts could, in principle, be realised by asymmetric SQUIDs providing a Josephson term $\sim -\cos(\phi + a\phi_{\text{ext}}) - \kappa\cos(\phi + [1-a]\,\phi_{\text{ext}}) = -A\cos(\phi+\delta)$, with $0<\kappa<1$ and $0<a<1$, as well as

$$\begin{aligned} A &= \pm\sqrt{[1-\kappa]^2 + 4\kappa\cos^2\left[\left(\frac{1}{2}-a\right)\phi_{\text{ext}}\right]}, \\ \delta &= \frac{\phi_{\text{ext}}}{2} - \arctan\left(\frac{1-\kappa}{1+\kappa}\tan\left[\left(\frac{1}{2}-a\right)\phi_{\text{ext}}\right]\right), \end{aligned} \tag{25}$$

where the sign of A follows that of the cosine. The π-shift can then be established in δ by inducing an external phase $\phi_{\text{ext}} \sim \pi/a$. It turns out that efficiency is maximal for $a=1$ (in which case ϕ_{ext} couples exclusively to the junction with the larger Josephson energy) and minimal for $a=0$ (where ϕ_{ext} couples only to the weaker junction). As discussed above, note that the parameter a, in general, depends on the device geometry and the magnetic field distribution of the external flux control hardware [60].

Note that the flux drive may in general not only couple to the Josephson junctions but also to the gyrators shunted in parallel. In accordance with Ref. [60], such a stray coupling can be neglected if the surface charges induced by the time-dependent flux drive (these are the charges screening the induced electric field) are mostly allocated near the junction. We expect this scenario to be plausible if junction and gyrator are sufficiently spatially separated with respect to the length scale on which the magnetic field varies. If such a spatial separation cannot be guaranteed, then one would have to take into account the microscopic and geometric details of the gyrator which is beyond the scope of this work.

To conclude this section, we point out similarities and differences to previous proposals creating analogue event horizons and Hawking radiation in solid state systems. Specifically, the analogue Hawking radiation previously predicted in Josephson junction arrays [33] relies on the creation of solitons, where within the finite extension of the soliton (over many lattice sites), the inductance can likewise be regarded as effectively negative within the soliton profile. The procedure we produce on the other hand involves creating $\pm\pi$ shifts on a connected series of junctions, which in essence corresponds to a tightly packed generation of "half"-solitons with the width of a single lattice site. Our system thus seems arguably much less stable. But first, as indicated already, the nonreciprocity provided by the gyrators allows for a stabilisation of the system even with inverted inductors, due to an extra (positive) inductive contribution. Second, the extra tilting mechanism provided by the gyrators allows for the explicit realisation of arbitrary (on-demand) spacetime geometries, and in addition, the

explicit creation of wormholes with (in principle) distinguishable black and white hole horizons. As for the evolution of the unstable system beyond transient times, we provide some thoughts in Sec. 6. Another important difference is that we here have in principle perfect control on the *position* of the horizon, contrary to the solitons studied in Ref. [32, 33], which are autonomously moving with respect to the lab frame. Moreover, we can create an event horizon with the precision of a single lattice site. This is in contrast to all other analogue Hawking radiation proposals (cold atoms, circuits, tilted Weyl semimetals), where the analogue metric always changes over a finite width (a healing length). This is an interesting caveat specifically regarding the existence of a well-defined Hawking temperature, or more generally, how to make sense of horizons with diverging surface gravity, as already indicated in Sec. 2.

5 Analogue horizons via flux quench

Once the optimisation problem of the current profile has been solved, the sign of the Josephson energy can be flipped for a region of the circuits described by the Hamiltonians (15) and (16), resulting in two horizons in the circuits (Fig. 2c).

The existence of tilted dispersion relations and horizons can be probed by means of injecting wave packets within the chains, and probe their time of flight. For example, within an overtilted region, wave packets can only move in one direction. At a white hole horizon, an incoming wave packet comes to a stand still. Such features represent a first experimentally available signature of the nontrivial spacetime geometry. Note that for the time evolution of the wave packets, the distinction between nearest and next-to-nearest neighbour coupling is not that important, under the condition that the experimenter is able to prepare wave packets close to $k \approx 0$ or $k \approx \pi$. These two types of excitations clearly distinguish between black and white hole horizon as they probe only a local part of k space. In addition, aspects of the wormhole stability (or instability) are not immediately visible in the wave packet amplitude (until the moment when the evaporation starts changing the spacetime geometry itself, see also Sec. 6 below).

We therefore present in addition a more sophisticated measurement which is able to probe radiation due to instabilities in a more direct fashion. Namely, this section examines how to characterise the system via two point charge and phase correlation functions. Additionally, two point correlation functions have been proposed and used to detect the presence of Hawking radiation in cold atom systems [41, 144], where they are directly related to the Hawking temperature. As foreshadowed above, while for a stable system, quantum fluctuations remain bounded over time, they start to diverge in the presence of complex eigenvalues. In the quadratic approximation, see Eq. (17), it is convenient to express the charge and phase operators for the circuits (15) and (16), in terms of bosonic operators

$$N_j = \frac{i}{\sqrt{2}}\left(a_j - a_j^\dagger\right), \tag{26}$$

$$\phi_j = \frac{1}{\sqrt{2}}\left(a_j + a_j^\dagger\right), \tag{27}$$

that obey the following commutation relations $[a_j, a_{j'}^\dagger] = \delta_{jj'}$, $[a_j, a_{j'}] = 0$. Now, calculating the two point correlation functions for charge and phase operators turns into calculating the correlation functions of the form $\langle a_j(t) a_{j'}^\dagger(t')\rangle$, $\langle a_j^\dagger(t) a_{j'}^\dagger(t')\rangle$, $\langle a_j(t) a_{j'}(t')\rangle$, and $\langle a_j^\dagger(t) a_{j'}(t')\rangle$.

We are going to calculate these correlations using two methods: 1) direct diagonalisation and 2) an extension of Klich's determinant formula [145]. The reason for the multi-pronged approach will be explained in detail below. To summarise, 1) is in principle very straightforward to implement and program, and is more versatile, as it would allow computing all types of observables, not only correlations. But diagonalisation is not applicable in the presence of

EPs, which is where method 2) comes into play, since it only requires exponentiation of the matrix with EPs.

As previously stated, once the system has been quenched, its state is in a highly excited state, were the new ground state is removed from the theory (a well-defined procedure for times sufficiently close to the quench). In order to anchor the theory to a well-defined ground state (necessary to compute observables in a well-defined way), we choose to perform computations with respect to the ground state of the unquenched system. Since the diagonalisation of the quenched Hamiltonian is being performed with respect to a state that is in general not its eigenstate, we will need a generalised version of bosonic Bogoliubov transformations. These transformations are discussed in Appendix B. We find that in presence of horizons, both kinds of circuits: one with nearest neighbour coupling via JJs and the other one with only next nearest neighbour coupling, give complex eigenvalues for the Bogoliubov transformations.

Implementing the Bogoliubov transformations on the quenched Hamiltonian, mentioned in the previous paragraph, requires diagonalising a non-Hermitian matrix. This can pose a problem if the matrix is defective (non-diagonalisable). One can, in principle, work with generalised eigenvectors, but this entails first determining whether the given matrix is diagonalisable or not, which is a numerically expensive procedure for large matrices and not very accurate if the eigenvalues are very close to each other. Additionally, working with generalised eigenvectors results in the Jordan normal form of the given matrix which is not diagonal for a defective matrix. We therefore suggest another method of calculating the correlations after the quench. Consider the following way to write a two point correlation

$$\left\langle a_i^\dagger(t)a_j(t)\right\rangle = \partial_\chi \left\langle e^{\chi a_i^\dagger(t)a_j(t)}\right\rangle_{\chi=0} = \lim_{\beta\to\infty} \frac{\mathrm{Tr}\left(e^{i\mathcal{H}_> t} e^{\chi a_i^\dagger a_j} e^{-i\mathcal{H}_> t} e^{-\beta\mathcal{H}_<}\right)}{\mathrm{Tr}\left(e^{-\beta\mathcal{H}_<}\right)}, \tag{28}$$

where $\mathcal{H}_<$ and $\mathcal{H}_>$ are the unquenched and quenched Hamiltonians, respectively. The many body traces in the above expression can be calculated by an extension of Klich's trace-determinant formula. The original formula was introduced to calculate the trace of many body operators by replacing it by a determinant of the corresponding first quantised operator [145]. The extension of this formula is described in appendices C and D. This approach bypasses the problem posed by defective eigenvalues but it is also considerably slower than diagonalisation for numerics, hence limiting the size of the systems we can work with. Another important remark: in the derivation (Appendix C) we have to assume the existence of a ground state for a non-Hermitian operator, which is not guaranteed. For some context about diagonalising quadratic bosonic non-Hermitian operators we also refer the reader to Ref. [146], where the concept of third quantisation [147] was extended to the bosonic Linblad equation. In Ref. [146], the existence of a ground state (or more appropriately, a non-equilibrium steady state) is always guaranteed due to the form of the Lindblad equation. Crucially, we do not have this constraint.

The system we will study here has hundred sites ($J = 100$) with the wormhole located between $j_0 = 30$ and $j_1 = 70$. For convenience, we impose periodic boundaries in position space (i.e., the 1D chain is closed into a loop). The parameters of the system are $|E_L'| = |E_L| = 3.42E_C$, $G = 2.4$ and $M = 3*10^{-4}E_C$. As already pointed out, in each of the following figures of correlation functions the result could be obtained by both diagonalisation and the generalised Klich determinant. The time steps in the following plots are $\delta t = 0.0031E_C^{-1}$ for the circuit with nearest neighbour coupling and $\delta t = 0.031E_C^{-1}$ for the next-to-nearest neighbour coupling.

First, let us examine the plots of correlation functions for the circuit with only nearest neighbour coupling, Fig. 6. We see that both phase and charge quantum fluctuations diverge after the quench. The system has two boundaries (red dotted lines) between the wormhole and the normal regions, that act as the horizons (located at j_0 and j_1). If we initialise low

energy excitations (for this circuit this means excitations near $k = 0$) in the region with overtilted dispersion, they move from the left horizon to the right horizon, hence we label them as the black and the white hole horizon respectively. The black hole horizon radiates away with time, as can be inferred by the accumulation of quantum fluctuations near it with time (which indicates presence of radiation), while the white hole horizon does not radiate. This explicitly confirms the previously discussed fact that for the nearest neighbour system, black and white hole horizons are distinguishable. The wormhole region also starts radiating due to the presence of the EP (as likewise already discussed in Sec. 3). We observe that the decay in the wormhole interior is much faster than the one induced by the presence of the horizons, which leads to the correlation functions growing much more rapidly *inside* the wormhole, before the black hole horizon show any appreciable decay. Overall, the above thus illustrates the possibility to create lattice simulations of wormholes with distinguishable black and white hole horizons, at the cost of a strong instability of the wormhole interior.

Now, let us focus on the circuit where Josephson junctions connect next nearest neighbours. Low-energy excitations in this circuit can be either near $k = 0$ or $k = \pm\pi$. For excitations (inside the wormhole region) near $k = 0$, similar to the previous circuit, the left boundary (j_0) acts as the black hole horizon and the right one (j_1) as the white hole. In contrast, for excitations near $k = \pm\pi$ the left boundary acts as the white hole horizon and right boundary as the black hole, hence we also refer to these as grey hole horizons. This symmetry is also reflected in the correlation plots in Fig. 7, where we can observe both horizons radiating away identically. Also, the only instability in this circuit is due to the horizons, leading to a much slower collapse.

An additional feature of the correlations of the phase difference, for this circuit, is the presence of oscillatory behaviour in the wormhole region (see Fig.(7a)). This behaviour is the consequence of the quench and is independent of the presence of the horizons. Hence, we can first look at the case of the translationally invariant quench, i.e. the case where all the inductors are flipped to have negative values and there are no horizons in the circuit. For this case we can write an analytical expression for $\left\langle \left(\phi_{j+1}(t) - \phi_{j-1}(t)\right)^2 \right\rangle$ and confirm that this oscillatory behaviour is indeed present. In general, this analytical expression contains a sum over many frequencies (number of frequencies $\sim J$), and any appearance of one single modulating frequency seems impossible. But, as J is increased we can approximate

$$\left\langle \left(\phi_{j+1}(t) - \phi_{j-1}(t)\right)^2 \right\rangle \approx A\cos\left(\omega_{\text{neg.}}\, t + \theta\right) + B, \tag{29}$$

where $\omega_{\text{neg.}} = 8\sqrt{E_C^2 G^2 - E_C E_L}$ and the values of A, B and θ depend on system parameters, we can verify this by looking at Fig. (8).

We can contrast above findings with a numerical calculation on a lattice with increasingly smooth variation of circuit parameters. Naively one would expect that there exists a continuum limit where the lattice theory maps back to the continuous Lagrangian (see Eq. (1)), where stable solutions exist (non-complex eigenvalues) and where horizons are unambiguously either black or white holes. Our calculation reveals the following (see Appendix E): while solutions with real-valued eigenfrequencies exist (reproducing thermal Hawking radiation) there remain two caveats. First of all the black/white hole ambiguity remains for the next nearest coupling model – giving rise to radiation close to both $k = 0$ and $k = \pi$ sectors. Secondly, the Boltzmann factor (expressing Hawking radiation) receives a renormalisation that depends strongly on the details of the discretisation, which likewise cannot be removed by simply letting the lattice constant go to zero. Overall, we can distinguish three types of field theories, which are all demonstrably distinct from one another. Lattice theories can either be considered in an unstable regime where parameters change abruptly with respect to the lattice constant, or a stable regime with smooth changes. However, even the latter does not simply map to the continuous model.

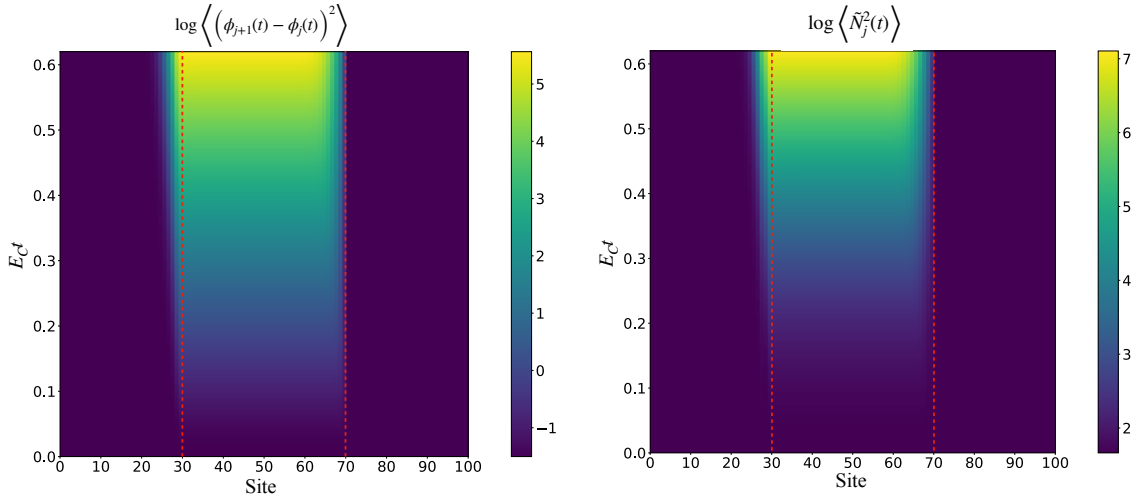

Figure 6: System with Josephson junctions connecting the nearest neighbours, (left) time evolution of quantum fluctuations of phase difference, (right) time evolution of quantum fluctuations of conjugate charge. Red dotted lines denote the position of the apparent horizons, i.e., boundaries between the wormhole and normal regions. Here, the fluctuations visibly distinguish between a pure black (pure white) hole horizon, where quantum fluctuations accumulate (or not). More over, the interior between the two horizons is here unstable, such that quantum fluctuations diverge immediately within the entire wormhole region.

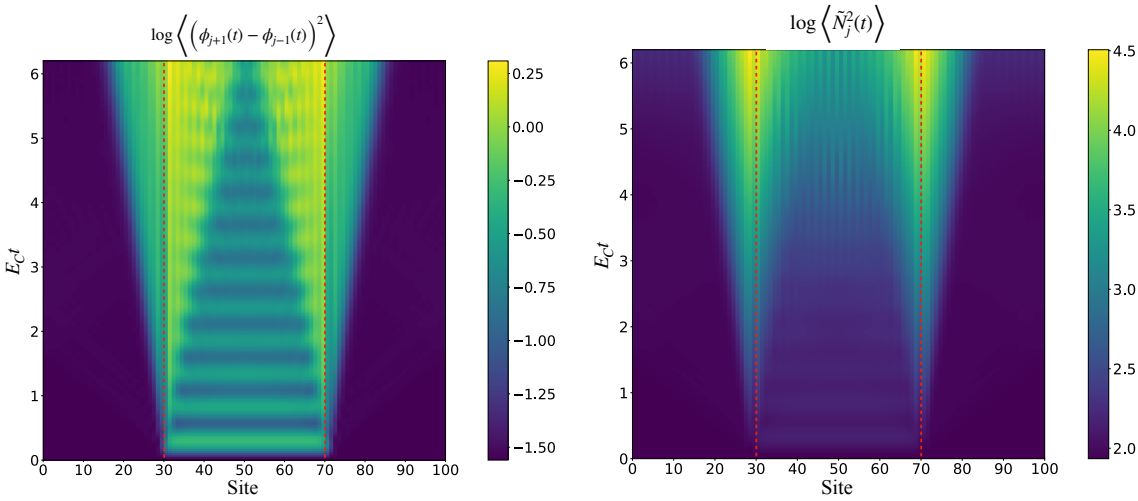

Figure 7: System with Josephson junctions connecting the next-nearest neighbours, (left) time evolution of quantum fluctuations of phase difference, (right) time evolution of quantum fluctuations of conjugate charge. Red dotted lines denote the position of the horizons. Here, (and contrary to Fig. 6) both horizons have black as well as white hole character, such that the two horizons are not easily distinguised when considering the spatial dependence of the fluctuations. On the other hand, the wormhole interior is here (at least initially) stable, and quantum fluctuations grow only from the horizons outwards.

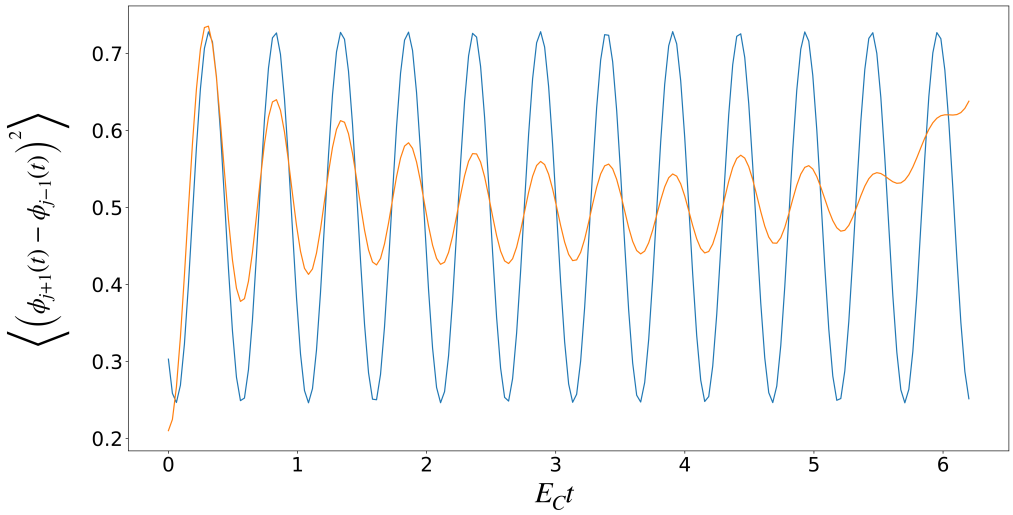

Figure 8: In the above figure, the orange line shows the time evolution of quantum fluctuations of phase differences in a circuit where JJs connect next nearest neighbours for $j = 50$, extracted from the data that is used to plot Fig. (7a). The blue line is the plot of the function $A\cos\left(\omega_{\text{neg.}}t + \theta\right) + B$, the values of A, B and θ have been hand fitted but in principle depend on the circuit parameters. We observe that $\omega_{\text{neg.}} = 8\sqrt{E_C^2 G^2 - E_C E_L}$ is a good approximation of the frequency of modulation obtained via numerics, until the evaporating horizons start affecting the site $j = 50$.

Lastly, we also investigated the effect of disorder in system parameters (specifically the gyrators and the inductors), on the behaviour of quantum fluctuations. Here, we summarise the results of this brief investigation, for the details see Appendix F:

- For the circuit with only nearest neighbour connections with small disorder (relative strength of disorder $\leq 5\%$), due to the fact that we don't see the disorder affecting the time evolution of quantum fluctuations in a significant manner (upper rows of Figs. (12) and (13)), we can conclude that the time scale associated with the effect of disorder is longer than the transient time during which we are calculating the time evolution of the quantum fluctuations.

- For the same circuit with large disorder (relative strength of disorder $\geq 10\%$), we do see some minor effect of disorder in the time evolution of quantum fluctuations in the wormhole region, but the effect on evaporation of the black hole horizon is still negligible (lower rows of Figs. (12) and (13)). Altogether, we can conclude that the effect of disorder on this circuit (for transient time) is not very significant.

- For the circuit with JJs connecting next nearest neighbours with relative disorder strength $\sim 5\%$, the time evolution of quantum fluctuations in the wormhole region already shows deviation form the case of no disorder (upper rows of Figs. (14) and (15)). But the evaporation of the two horizons remains qualitatively unaffected.

- For the same circuit with large disorder, the time evolution of quantum fluctuations and the evaporation of the two horizons is significantly different from the case of no disorder (lower rows of Figs. (14) and (15)), hence the time scale of large disorder is comparable to the transient time for this circuit.

- For the second circuit we impose the condition $4G^2 > E_L/E_C$ on the parameters, combining this fact with the low energy dispersion relation in Eq.(20) we can expect the disorder

in gyrators to be more significant than the disorder in inductors. Comparing the effect of disorder in gyrators and inductors, plotted in Figs. (14) and (15) respectively, confirms this expectation.

6 Perspective on wormhole evaporation over long times

As shown in the previous section, charge and phase fluctuations accumulate very rapidly due to the fundamental instability inherent to the wormhole horizons or interior (in case of nearest neighbour inductive coupling) – an effect distinct from regular Hawking radiation. In particular, the more the system accumulates charge and phase fluctuations over time, the more the quadratic approximation of the Josephson energy becomes inaccurate, such that predicting the system dynamics for long times becomes a much harder task (as the system can no longer be approximated by non-interacting bosons). This is well beyond the scope of the present work. We nonetheless find it illustrative to speculate on a qualitative level about the long term fate of the wormhole – especially as it allows us to distinguish between intrinsic (spontaneous) collapse, and dissipative relaxation. In addition, some of the resulting concepts provide an interesting segue to the subsequent idea: quantum superpositions of the spacetime geometry.

To this end, let us take into account interactions with an environment. For the sake of simplicity and concreteness, we consider the phase difference $\phi_j - \phi_{j-1} + \phi_{\text{ext},j}$ across a single junction. At the beginning of the wormhole quench, this phase difference is either localised around 0 (minimum of the cosine, if the junction is positioned outside the wormhole) or around $\pm\pi$ (maximum of the cosine, inside the wormhole). In the presence of the instability, the quantum fluctuations of this phase difference blow up over time, as shown in the previous section. Now suppose that the environment entangles (either weakly or strongly) with the current across this junction. This means that the phase difference gets spontaneously projected onto a more localised state. Notably, this type of environment-induced process thus *diminishes* quantum fluctuations. We note that the same picture holds in perfect analogy for the accumulation of charge noise quantum fluctuations, respectively, the reduction thereof by a dissipative process extracting information about the charge.

To proceed, note that the location of the wave function now is no longer at 0 or π, but can be (with a finite probability) at a certain distance from the minimum or maximum. With the new location updated, we again quadratically expand the cosine around the new peak position of the phase difference. Importantly, due to the cosine behaviour of the junction the resulting effective inductance is now different (the curvature of the cosine obviously changes as a function of the position at which it is calculated). Thus, as time progresses, and the phase difference starts to classically diffuse after repeated environment-induced measurements, the effective inductance at a given junction likewise fluctuates classically. At this point, the impact of such dissipative processes could likewise be detectable in time-of-flight measurements of wave packets within the array. At any rate, the most likely long-term outcome is that all phase differences relax to the ground state, equivalent to the complete evaporation of the analogue wormhole. We note that for a system on a ring (with periodic boundaries), or a system with a finite mass term (Cooper-pair leakage to ground), the emergence of soliton states might be a possibility.

Let us repeat that even though the environment will undoubtedly have a big impact on the system dynamics (especially beyond the immediate transient time scale), the experimental signatures of *quantum collapse* (due to complex eigenvalues) and *classical collapse* (due to dissipation) could not be more different. The instability due to the inhomogeneous metric leads to an increase of *quantum* fluctuations, whereas the environment induces *classical* fluctuations. Thus, the observation of the former can distinguish between how the system intrinsically reacts to the creation of an instability, as compared to the impact of external perturbations.

To conclude this section, we consider the very hypothetical case of negligible coupling to the environment, as it reveals an interesting additional idea which we hope to pursue in future works. If we assume that the build-up of quantum fluctuations of the phase could progress unimpeded over longer times, the non-linearity of the Josephson energies results not in classical fluctuations of the effective inductance (as in the previous paragraph), but in a system that can be interpreted as being in a *quantum* superposition of different effective inductances – a form of quantum superposition of the spacetime geometry itself. However, within the above considered setting, this effect will likely not survive for very long times due to environment-induced decoherence of the quantum fluctuations, and even for a highly protected system, it would be hard to analyse the effect in an unambiguous way. In upcoming papers, we plan to provide a modification of this idea, not relying on instabilities (and thus not requiring any ultra-fast quenches), but instead on more general notions of Josephson junctions with multiple minimas, so-called multi-stable Josephson junctions [118–120]. This endeavour will on the one hand introduce the notion of a quantum inductance, and with it, a likely more stable version of a quantum superposition of the analogue spacetime. As we will show, there exist protocols allowing classical signals to entangle with quantum spacetime, marking a highly non-trivial form of backaction between fields and the spacetime they traverse.

7 Conclusions and outlook

In this paper we have proposed using quantum circuits to implement analogue event horizons on a discrete lattice. Even though this idea is a well explored concept in solid state systems in general, we here explicitly demonstrate the capacity of superconducting circuits to emulate arbitrary spacetime configurations. By identifying a minimal fundamental set of necessary circuit elements, we further unravel a number of surprising findings pertinent to lattice systems, which allow in particular to create horizons where the change in metric parameters happens at a level of a single lattice site. To implement analogue horizons in a quantum circuit, we proposed a general way of creating negative inductances with Josephson junctions transiently driven by nearby current loops. We further uncovered two subtly distinct ways to engineer a region with overtilted dispersion relation, either with inductive coupling of nearest or next-to-nearest neighbour nodes. While for the latter, horizons have a grey hole character (as is the most usual case in lattices), the former [Eq. (15)] hosts two distinct kinds of horizons, one that acts purely as a black hole horizon and the other as a white hole horizon. For this second type of circuit, it is not only the horizons, but also the region between the horizons (wormhole interior) that is unstable due to the presence of an EP. This instability also contributes to the observed radiation (in addition to the evaporation of the horizons) as can be confirmed by tracking the quantum fluctuations of phase difference and conjugate charge with time (Fig. 6). In addition to Bogoliubov diagonalisation, we used an extension of Klich's trace-determinant formula to obtain the correlation functions numerically. The proof of this extension remains elusive for a general operator, but in the parameter regime where the generalised Bogoliubov transformation is applicable, the results of both numerical methods agree.

In this paper, in addition to standard circuit elements, we have also included elements that are still being developed experimentally (such as quantum gyrators), or introduced new effective circuit elements (negative inductors based on regular Josephson junctions), which, even though experimentally tested in existing works, are here proposed to be operated in previously unexplored regimes. We here therefore point at feasible small scale experimental tests that can act as proofs of principle for the basic physical principles behind the considered physics. For instance, our proposal of using current loops to invert the effective inductance of a Josephson junction can be tested on a single transmon, where the qubit frequency becomes imaginary $\sqrt{E_J E_C} \to \sqrt{-E_J E_C}$ for transient times. The resulting accumulation of phase or

charge quantum fluctuations (or limits thereof due to coupling to the environment) can thus be tested in an "imaginary" qubit device. Such a study might be also of some fundamental interest, when extending the description of the junction beyond the quadratic approximation, where the expansion around the energy minimum or the energy maximum can be regarded as real and imaginary twins of nonlinear dynamics – ready to be explored in future works. This work also serves as a motivation for exploring more ambitious theoretical ideas, such as the inclusion of higher order terms in the expansion of the cosine. For example, if we expand the cosine up to the quartic term $\sim \phi_j^4$, the result would be an interacting scalar field theory. Such an investigation will be crucial in extending the capabilities of circuit QED to simulate more complex light-matter interactions. Additionally, as alluded to in Sec. 6, another extension of the present work is the study of backaction of quantum fields on spacetime geometry. This follows from the fact that the emergent spacetime geometry in this manuscript depends on the curvature of the Josephson potential at its minima i.e. the effective inductance. As the wave function of the system, initially located at the maxima of the inverted Josephson potential, evolves in time it will experience different curvatures of the potential and hence different effective inductances. Therefore, the state of the system will determine the emergent spacetime geometry, and this emergent spacetime geometry in turn will affect the evolution of the system. For obvious reasons this is a very complicated problem to solve, suitable for follow-up research.

Acknowledgments

We acknowledge interesting and fruitful discussions with Zaki Leghtas, Roudy Hanna, Philippe Campagne-Ibarcq and David DiVincenzo.

Funding information This work has been funded by the German Federal Ministry of Education and Research within the funding program Photonic Research Germany under the contract number 13N14891.

A Josephson junction array with gyrators

Here we solve a JJ array with gyrators

$$\mathcal{H} = E_C \sum_{j=1}^{J} \Big[N_j + G(\phi_{j+1} - \phi_{j-1}) \Big]^2 + E_L \left(\phi_{j+1} - \phi_j\right)^2 + M\phi_j^2 \,, \tag{A.1}$$

and periodic boundary conditions, where we have introduced a mass term to regularize the zero mode. Define the Fourier transform as follows

$$\begin{aligned} N_k &= \frac{1}{\sqrt{J}} \sum_{j=1}^{J} e^{ik_m j} N_j \,, \\ \phi_k &= \frac{1}{\sqrt{J}} \sum_{j=1}^{J} e^{-ik_m j} \phi_j \,, \\ k_m &= \frac{2\pi m}{J} \,, \end{aligned} \tag{A.2}$$

where $m \in \{-J/2+1, -J/2+2, ..., J/2\}$. The Hamiltonian can now be written as

$$\mathcal{H} = E_C \sum_{m=-\frac{J}{2}+1}^{\frac{J}{2}} \left[N_m N_{-m} + i2G \sin\left(\frac{2\pi m}{J}\right) \{N_m, \phi_m\} + \beta_m \phi_m \phi_{-m} \right] , \tag{A.3}$$

where

$$\beta_m = \frac{4E_C G^2 \sin^2\left(\frac{2\pi m}{J}\right) + 4E_L \sin^2\left(\frac{\pi m}{J}\right) + M}{E_C},$$

and $\{\cdot,\cdot\}$ denotes the anti-commutator. Now, we write the Fourier transformed charge and phase operators in terms of bosonic annihilation and creation operators

$$N_m = \frac{i}{\sqrt{2}}\left(a_{-m} - a_m^\dagger\right), \tag{A.4}$$

$$\phi_m = \frac{1}{\sqrt{2}}\left(a_m + a_{-m}^\dagger\right), \tag{A.5}$$

that obey the following commutation relations $[a_m, a_{m'}^\dagger] = \delta_{mm'}$, $[a_m, a_{m'}] = 0$. Finally, the Hamiltonian becomes

$$\begin{aligned}\mathcal{H} = &\frac{E_C}{2}\sum_{m=1}^{\frac{J}{2}-1}\begin{pmatrix} a_m^\dagger & a_{-m}^\dagger & a_m & a_{-m}\end{pmatrix} H_{1,m}\begin{pmatrix} a_m \\ a_{-m} \\ a_m^\dagger \\ a_{-m}^\dagger\end{pmatrix} \\ &+ \frac{E_C}{2}\begin{pmatrix} a_0^\dagger & a_0\end{pmatrix} h \begin{pmatrix} a_0 \\ a_0^\dagger\end{pmatrix} + \frac{E_C}{2}\begin{pmatrix} a_{\frac{J}{2}}^\dagger & a_{\frac{J}{2}}\end{pmatrix} h' \begin{pmatrix} a_{\frac{J}{2}} \\ a_{\frac{J}{2}}^\dagger\end{pmatrix}, \\ \mathcal{H} = &\sum_{m=1}^{\frac{J}{2}-1}\mathcal{H}_{1,m} + \mathcal{H}_2 + \mathcal{H}_3,\end{aligned} \tag{A.6}$$

where

$$H_{1,m} = (\beta_m + 1)\mathbb{I}_4 + 4G\sin\left(\frac{2\pi m}{J}\right)\begin{pmatrix}\sigma_z & 0 \\ 0 & \sigma_z\end{pmatrix} + (\beta_m - 1)\begin{pmatrix} 0 & \sigma_x \\ \sigma_x & 0\end{pmatrix}, \tag{A.7}$$

$$h = (\beta_0 + 1)\mathbb{I}_2 + (\beta_0 - 1)\sigma_x, \tag{A.8}$$

$$h' = \left(\beta_{\frac{J}{2}} + 1\right)\mathbb{I}_2 + \left(\beta_{\frac{J}{2}} - 1\right)\sigma_x. \tag{A.9}$$

$\mathbb{I}_n$ is a n-dimensional identity matrix while σ_z and σ_x are Pauli matrices. We will focus on diagonalisation of $\mathcal{H}_{1,m}$ in eq.(A.6), the same formalism can be used for the other parts.

We will use the diagonalisation of $\mathcal{H}_{1,m}$ to outline some general properties of a Bosonic Bogoliubov transformation. Our goal is to find new operators, $b_m, b_m^\dagger$ such that

$$\mathcal{H}_{1,m} = \frac{E_C}{2}\begin{pmatrix} b_m^\dagger & b_{-m}^\dagger & b_m & b_{-m}\end{pmatrix}\tau_z \Lambda_m \begin{pmatrix} b_m \\ b_{-m} \\ b_m^\dagger \\ b_{-m}^\dagger\end{pmatrix}, \tag{A.10}$$

where Λ_m is a diagonal matrix, and the new operators still satisfy the Bosonic commutation relations. This entails finding a matrix Q_m such that

$$\Lambda_m = Q_m^{-1}\tau_z H_m Q_m, \tag{A.11}$$

where

$$\tau_z = \begin{pmatrix}\mathbb{I}_2 & 0 \\ 0 & -\mathbb{I}_2\end{pmatrix}.$$

Since the column vector and the row vector in eq.(A10) are related by Hermitian conjugation, this imposes the following condition

$$Q_m^{-1} = \tau_z Q_m^\dagger \tau_z \,. \tag{A.12}$$

Moreover the column (and the row) in eq.(A10) has internal structure as well, the bottom half of the column contains Hermitian conjugates of the upper half, this results in the following conditions

$$Q_m^* = \tau_x Q_m \tau_x \,, \tag{A.13}$$
$$\Lambda_m = -\tau_x \Lambda_m \tau_x \,, \tag{A.14}$$

where

$$\tau_x = \begin{pmatrix} 0 & \mathbb{I}_2 \\ \mathbb{I}_2 & 0 \end{pmatrix}.$$

Finally, we can write

$$\begin{aligned} \mathcal{H}_{1,m} &= \frac{E_C}{2} \begin{pmatrix} a_m^\dagger & a_{-m}^\dagger & a_m & a_{-m} \end{pmatrix} \tau_z Q_m \tau_z \tau_z \Lambda_m Q_m^{-1} \begin{pmatrix} a_m \\ a_{-m} \\ a_m^\dagger \\ a_{-m}^\dagger \end{pmatrix} \\ &= \frac{E_C}{2} \begin{pmatrix} b_m^\dagger & b_{-m}^\dagger & b_m & b_{-m} \end{pmatrix} \tau_z \Lambda_m \begin{pmatrix} b_m \\ b_{-m} \\ b_m^\dagger \\ b_{-m}^\dagger \end{pmatrix}. \end{aligned} \tag{A.15}$$

The above procedure of Bogoliubov transformation is only applicable if Λ_m is a real matrix, for complex matrix we will develop the procedure in the next section.

The complete diagonalised Hamiltonian is

$$\mathcal{H} = \sum_{m=-\frac{J}{2}+1}^{\frac{J}{2}} \omega_m b_m^\dagger b_m \,, \tag{A.16}$$

$$\omega_m = 2\sqrt{E_C^2 \beta_m} + 4E_C G \sin\left(\frac{2\pi m}{J}\right). \tag{A.17}$$

We also investigate the arrays where the Josephson junction connects next nearest neighbours, the Hamiltonian for such a system will be

$$\mathcal{H}' = E_C \sum_{j=1}^{J} \left[N_j + G(\phi_{j+1} - \phi_{j-1})\right]^2 + E_L \left(\phi_{j+1} - \phi_{j-1}\right)^2 + M\phi_j^2 \,. \tag{A.18}$$

This Hamiltonian can be diagonalised in a similar way to get

$$\begin{aligned} \mathcal{H}' &= \sum_{m=-\frac{J}{2}+1}^{\frac{J}{2}} \omega_m b_m^\dagger b_m \,, \\ \omega_m &= 2\sqrt{E_C^2 \beta_m} + 4E_C G \sin\left(\frac{2\pi m}{J}\right), \\ \beta_m &= \frac{4\left(E_C G^2 + E_L\right)\sin^2\left(\frac{2\pi m}{J}\right) + M}{E_C} \,. \end{aligned} \tag{A.19}$$

B Bogoliubov transformation for calculating correlations after quench

Consider the following Hamiltonian

$$\mathcal{H} = E_C \sum_{j=1}^{J} \Big[N_j + G(\phi_{j+1} - \phi_{j-1}) \Big]^2 + E_{L,j} \left(\phi_{j+1} - \phi_j \right)^2 + M \phi_j^2 \,. \tag{B.1}$$

The term $E_{L,j}$ indicates that the inductance can vary with site. Since there is no translational invariance, we cannot use Fourier transform, instead we write the phase and charge operators in terms of Bosonic annihilation and creation operators

$$N_j = \frac{i}{\sqrt{2}} \left(a_j - a_j^\dagger \right), \tag{B.2}$$

$$\phi_j = \frac{1}{\sqrt{2}} \left(a_j + a_j^\dagger \right), \tag{B.3}$$

that obey the following commutation relations $[a_j, a_{j'}^\dagger] = \delta_{jj'}$, $[a_j, a_{j'}] = 0$. This allows us to write the Hamiltonian as

$$\mathcal{H} = \mathbf{a}^\dagger H \mathbf{a} \,, \tag{B.4}$$

where $\mathbf{a} = \begin{pmatrix} a_1 & \cdots & a_J & a_1^\dagger & \cdots & a_J^\dagger \end{pmatrix}^T$.

We begin with the unquenched Hamiltonian, where $E_{L,j} = E_L$, this is the same Hamiltonian that we solved in appendix A, this time in position space, we can still follow the same steps and diagonalise it without going to the Fourier space to get

$$\begin{aligned} \mathcal{H}_< &= \mathbf{a}^\dagger H_< \mathbf{a} \\ &= \mathbf{a}^\dagger Z Q Z Z \Lambda_< Q^{-1} \mathbf{a} \\ &= \mathbf{b}^\dagger Z \Lambda_< \mathbf{b} \\ &= \sum_{j=1}^{J} \left(\lambda_{<,j} b_j^\dagger b_j + \lambda_{<,j} b_j b_j^\dagger \right). \end{aligned} \tag{B.5}$$

Here

$$Z = \begin{pmatrix} \mathbb{I}_J & 0 \\ 0 & -\mathbb{I}_J \end{pmatrix},$$

and operators $\mathbf{b}^{(\dagger)}$ have the same commutation relations as $\mathbf{a}^{(\dagger)}$. The matrix Q satisfies the conditions in Eq. (A.12) and (A.13), while the diagonal matrix $\Lambda_<$ satisfies the Eq. (A.14). In position space the Hamiltonian does not break down into independent blocks of 4×4 matrices, therefore the size of the matrices in the above equations have to be changed appropriately.

Now we quench the system such that

$$E_{L,j} = \begin{cases} -E_L \,, & j_0 < j < j_1 \,, \\ E_L \,, & \text{everywhere else,} \end{cases} \tag{B.6}$$

for some arbitrary j_0 and j_1. The quenched Hamiltonian can be written as

$$\begin{aligned} \mathcal{H}_> &= \mathbf{a}^\dagger H_> \mathbf{a} \\ &= \mathbf{a}^\dagger Z P Z Z \Lambda_> P^{-1} \mathbf{a} \,. \end{aligned} \tag{B.7}$$

The diagonal matrix $\Lambda_>$ is not necessarily real, therefore the Eq. (A.12) and (A.13) doesn't hold, but these conditions translate to conditions on the first quantised matrix as

$$\begin{aligned} H_> &= H_>^\dagger , \\ H_>^T &= X H_> X , \\ X &= \begin{pmatrix} 0 & \mathbb{I}_J \\ \mathbb{I}_J & 0 \end{pmatrix} , \end{aligned} \tag{B.8}$$

which still hold true. From this we can get some new properties

$$P^{-1} = ZXP^T XZ , \tag{B.9}$$

$$\Lambda_> = -X\Lambda_> X , \tag{B.10}$$

$$\Lambda_> = M^{-1}\Lambda_>^* M , \tag{B.11}$$

where $M = ZP^\dagger ZP$. One might notice that Eq. (B.9) is just the combination of Eq. (A.12) and (A.13). The unquenched Hamiltonian can now be written as

$$\begin{aligned} \mathcal{H}_> &= \mathbf{c}^\bullet Z_{2J} \Lambda_> \mathbf{c} \\ &= \sum_{j=1}^{J} \left(\lambda_{>,j} c_j^\bullet c_j + \lambda_{>,j} c_j c_j^\bullet \right) , \end{aligned} \tag{B.12}$$

where

$$\begin{aligned} \mathbf{c}^\bullet &= \begin{pmatrix} c_1^\bullet & \cdots & c_J^\bullet & c_1 & \cdots & c_J \end{pmatrix} , \\ \mathbf{c} &= \begin{pmatrix} c_1 & \cdots & c_J & c_1^\bullet & \cdots & c_J^\bullet \end{pmatrix}^T . \end{aligned}$$

The new operators obey the following commutation relations $[c_j, c_{j'}^\bullet] = \delta_{jj'}$, $[c_j, c_{j'}] = 0$, $[c_j^\bullet, c_{j'}^\bullet] = 0$. These relations closely resemble Bosonic commutation relations, but it is important to note that the operators $c_j^\bullet$ and c_j are not related by Hermitian conjugation.

Any two point correlation of charge and phase operators can be written as a linear combination of two point correlators of the $\mathbf{a}^{(\dagger)}$ operators, hence we focus on finding the following correlation matrix

$$F(t,t') \equiv \left\langle \mathbf{a}(t)\mathbf{a}^\dagger(t') \right\rangle , \tag{B.13}$$

where the average is taken over the ground state of the equilibrium system. For a total number of J sites F is a $2J \times 2J$ matrix with the substructure form

$$F(t,t') = \begin{pmatrix} A(t,t') & B(t,t') \\ C(t,t') & D(t,t') \end{pmatrix} , \tag{B.14}$$

where A, B, C and D are block matrices of dimensions $J \times J$ that contain the correlations of the form $\left\langle a_j(t) a_{j'}^\dagger(t') \right\rangle$,$\left\langle a_j^\dagger(t) a_{j'}^\dagger(t') \right\rangle$,$\left\langle a_j(t) a_{j'}(t') \right\rangle$ and $\left\langle a_j^\dagger(t) a_{j'}(t') \right\rangle$ respectively.

First let us calculate the correlation matrix for unquenched Hamiltonian

$$F_<(t,t') = Q \left\langle \mathbf{b}(t)\mathbf{b}^\dagger(t') \right\rangle ZQ^{-1}Z . \tag{B.15}$$

In this step we have used the fact that the matrices Q and Z_{2J} commute with many-body operator $\mathcal{H}_<$. Since the ground state of unquenched Hamiltonian is defined as $b_i |0\rangle = 0 \ \forall i$, we get

$$F_<(t,t') = Q e^{-i2(t-t')\Lambda_<} \frac{\mathbb{I}_{2J} + Z}{2} Q^{-1} Z . \tag{B.16}$$

Now we focus on the case where we quench the system. Namely, we prepare the system in a ground state of a different Hamiltonian $\mathcal{H}_<$ for times $t<0$, and immediately switch the system to the Hamiltonian $\mathcal{H}_>$ at time $t=0$ (and let it evolve for subsequent $t>0$). Using the previous results we can finally write down the correlation matrix

$$\begin{aligned}
F_>(t,t') &= \left\langle \mathbf{a}(t)\mathbf{a}^\dagger(t')\right\rangle \\
&= P\left\langle \mathbf{c}(t)\mathbf{c}^\bullet(t')\right\rangle ZP^{-1}Z \\
&= Pe^{-i2\Lambda_> t}\left\langle \mathbf{c}\mathbf{c}^\bullet\right\rangle e^{i2\Lambda_> t'}ZP^{-1}Z \\
&= Pe^{-i2\Lambda_> t}P^{-1}\left\langle \mathbf{a}\mathbf{a}^\dagger\right\rangle ZPe^{i2\Lambda_> t'}P^{-1}Z \\
&= Pe^{-i2\Lambda_> t}P^{-1}Q\left\langle \mathbf{b}\mathbf{b}^\dagger\right\rangle ZQ^{-1}Pe^{i2\Lambda_> t'}P^{-1}Z \\
&= Pe^{-i2\Lambda_> t}P^{-1}Q\frac{\mathbb{I}_{2J}+Z}{2}Q^{-1}Pe^{i2\Lambda_> t'}P^{-1}Z \\
&= e^{-i2H_> t}Q\frac{\mathbb{I}_{2J}+Z}{2}Q^{-1}e^{i2H_> t'}Z\,.
\end{aligned} \tag{B.17}$$

C Klich's determinant formula

Consider two second quantised operators $\hat{A}$ and $\hat{B}$, such that

$$\begin{aligned}
\hat{A} &= \sum_{i,j}\langle i|A|j\rangle\, d_i^\dagger d_j\,, \\
\hat{B} &= \sum_{i,j}\langle i|B|j\rangle\, d_i^\dagger d_j\,,
\end{aligned}$$

where A and B are first the quantised operators and the states $|i\rangle$ span the corresponding single particle Hilbert space. Then it can be shown that [145]

$$\mathrm{Tr}\left(e^{\hat{A}}e^{\hat{B}}\right) = \det\left(1-\xi e^A e^B\right)^{-\xi}\,, \tag{C.1}$$

where $\xi=1$ for Bosons and $\xi=-1$ for Fermions (the creation and annihilation operators satisfy $d_i d_j^\dagger - \xi d_j^\dagger d_i = \delta_{ij}$).

We are going to derive a similar formula for operators that also contain terms of the form $d_i d_j$ and $d_i^\dagger d_j^\dagger$, we will work with Bosonic operators, the formula for Fermionic operators can be derived in a similar way.

Consider an operator (not necessarily Hermitian) that can be written in terms of Bosonic creation and annihilation operators as follows

$$\hat{A} = \sum_{i,j=1}^{J} a_i^\dagger A^{(0)}_{ij} a_j + \frac{1}{2}a_i^\dagger A^{(1)}_{ij}a_j^\dagger + \frac{1}{2}a_i A^{(2)}_{ij}a_j = \frac{1}{2}\mathcal{A} - \frac{1}{2}\mathrm{tr}A^{(0)} \tag{C.2}$$

(note: Tr is the trace for a many body operator while tr is the normal trace for a matrix), here

$$\begin{aligned}
\mathcal{A} &= \mathbf{a}^\dagger A\mathbf{a}\,, \\
A &= \begin{pmatrix} A^{(0)} & A^{(1)} \\ A^{(2)} & A^{(0)T}\end{pmatrix}.
\end{aligned}$$

The matrices $A^{(1)}$ and $A^{(2)}$ can always be written as symmetric matrices due to the Bosonic commutation relations. This leads to the following property

$$XAX = A^T\,. \tag{C.3}$$

To calculate the trace of this many body operator, we can diagonalise ZA but since it is not Hermitian, there is no guarantee that it is diagonalisable. Instead we find Schur's decomposition of ZA i.e.

$$ZA = U\Lambda U^\dagger\,, \tag{C.4}$$

where U is a unitary matrix and Λ is an upper triangular matrix with eigenvalues of ZA on its diagonal. Schur's decomposition allows us to arrange the eigenvalues in any order we want on the diagonal of Λ, we will choose the following arrangement

$$\mathrm{Diag}\Lambda = \begin{pmatrix} \lambda_1 & \cdots & \lambda_J & -\lambda_J & \cdots & -\lambda_1 \end{pmatrix}, \tag{C.5}$$

the above arrangement is possible because the eigenvalues of ZA come in pairs of $(\lambda, -\lambda)$, this fact can be ascertained from the following property

$$\begin{aligned} &\text{if} \quad (ZA-\lambda)^m |\lambda\rangle = 0 \\ \implies &|\lambda\rangle^T ZX\,(ZA+\lambda)^m = 0\,, \end{aligned} \tag{C.6}$$

for $m \geq 1$, the $m \neq 1$ cases correspond to generalised eigenvectors. The specific arrangement of eigenvalues in Eq. (C.5) also imposes a specific structure on the matrix U, which is

$$U = \begin{pmatrix} |\lambda_1\rangle & \cdots & |\lambda_J\rangle & XZ\,|\lambda_J\rangle^* & \cdots & XZ\,|\lambda_1\rangle^* \end{pmatrix}, \tag{C.7}$$

where $|\lambda_i\rangle$ is the (generalised) eigenvector corresponding to the eigenvalue λ_i. The eigenvectors are normalized as follows

$$|\lambda_i\rangle^\dagger \left|\lambda_j\right\rangle = \delta_{ij}\,. \tag{C.8}$$

Now we return to the problem of calculating the trace of the many body operator, for that

$$\begin{aligned} \mathcal{A} &= \mathbf{a}^\dagger A \mathbf{a} \\ &= \mathbf{a}^\dagger ZUZZ\Lambda U^\dagger \mathbf{a} \\ &= \begin{pmatrix} c_1^\bullet & \cdots & c_J^\bullet & c_J & \cdots & c_1 \end{pmatrix} Z\Lambda \begin{pmatrix} c_1 & \cdots & c_J & c_J^\bullet & \cdots & c_1^\bullet \end{pmatrix}^T, \end{aligned} \tag{C.9}$$

and the commutation relations for the new operators are $[c_j, c_{j'}^\bullet] = \delta_{jj'}$, $[c_j, c_{j'}] = 0$, $[c_j^\bullet, c_{j'}^\bullet] = 0$. Finally,

$$\mathcal{A} = \sum_{i=1}^{J} \lambda_i \left(c_i^\bullet c_i + c_i c_i^\bullet\right) + \sum_{i,j=1}^{J} N_{ij} c_i^\bullet c_j^\bullet + \sum_{i<j,i=1}^{J} R_{ij} c_i^\bullet c_j\,, \tag{C.10}$$

where the terms N_{ij} and R_{ij} encompass the non-diagonal terms of the upper triangular matrix Λ.

Define two states $\langle 0|_L$ and $|0\rangle_R$ such that

$$\langle 0|_L\, c_i^\bullet = 0 \;\forall i\,, \tag{C.11}$$

$$c_i\,|0\rangle_R = 0 \;\forall i\,. \tag{C.12}$$

Then it is easy to see that the operator $\sum_{i=1}^{J} c_i^\bullet c_i$ acts as a number operator. We can define a basis for a Fock space in terms of the following states

$$|n_1, n_2, \cdots, n_J\rangle = \frac{c_1^{\bullet n_1} c_2^{\bullet n_2} \cdots c_J^{\bullet n_J}}{\sqrt{n_1! n_2! \cdots n_J!}}\,|0\rangle_R\,, \tag{C.13}$$

$$\langle\langle n_1, n_2, \cdots, n_J| = \langle 0|_L \frac{{c_1}^{n_1} {c_2}^{n_2} \cdots {c_J}^{n_J}}{\sqrt{n_1! n_2! \cdots n_J!}}\,. \tag{C.14}$$

The states are normalized such that

$$\langle\langle n_1, n_2, \cdots, n_J| \, |m_1, m_2, \cdots, m_J\rangle = \delta_{n_1,m_1}\delta_{n_2,m_2}\cdots\delta_{n_J,m_J}\,, \tag{C.15}$$

and the resolution of the identity on the Fock space is

$$\hat{\mathcal{I}} = \sum_{n_1=0}^{\infty}\cdots\sum_{n_J=0}^{\infty} |n_1, n_2, \cdots, n_J\rangle\,\langle\langle n_1, n_2, \cdots, n_J| \,. \tag{C.16}$$

The trace of the exponential of the many body operator can now be written as

$$\begin{aligned}
\mathrm{Tr}e^{\hat{A}} &= e^{-\mathrm{tr}A^{(0)}/2}\mathrm{Tr}e^{\mathcal{A}/2} \\
&= e^{-\mathrm{tr}A^{(0)}/2}\sum_{n_1=0}^{\infty}\cdots\sum_{n_J=0}^{\infty}\langle\langle n_1, n_2, \cdots, n_J|\, e^{\mathcal{A}/2}\,|n_1, n_2, \cdots, n_J\rangle \\
&= \sum_{n_1=0}^{\infty}\cdots\sum_{n_J=0}^{\infty}\langle\langle n_1, n_2, \cdots, n_J|\, e^{\sum_{i=1}^{J}\lambda_i\left(c_i^{\bullet}c_i + c_i c_i^{\bullet}\right)/2}\,|n_1, n_2, \cdots, n_J\rangle \\
&= \prod_{i=1}^{J}\frac{e^{\lambda_i/2}}{1-e^{\lambda_i}}\,.
\end{aligned} \tag{C.17}$$

The terms $\sum_{i,j=1}^{J} N_{ij}c_i^{\bullet}c_j^{\bullet}$ and $\sum_{i<j,i=1}^{J} R_{ij}c_i^{\bullet}c_j$ change the number states in such a way that no combination of them with each other or themselves can contribute to the trace, therefore the only term that contributes is $\sum_{i=1}^{J}\lambda_i\left(c_i^{\bullet}c_i + c_i c_i^{\bullet}\right)$. This was the reason why we chose a specific arrangement of eigenvalues in Eq. (C.5).

We can write eq.(C18) as

$$\mathrm{Tr}e^{\hat{A}} = e^{-\mathrm{tr}A^{(0)}/2}\det(1-UU^{\dagger}Ze^{ZA/2})^{-1}\,, \tag{C.18}$$

which doesn't appear to be universal on account of the appearance of the matrix U, instead we will work with the following formula

$$\left[\mathrm{Tr}e^{\hat{A}}\right]^2 = \det(Z)e^{-\mathrm{tr}A^{(0)}}\det(1-e^{ZA})^{-1}\,. \tag{C.19}$$

We still don't have an expression which is analogous to the Eq. (C.1), to derive such an expression, consider another operator $\hat{B}$ that can be written in a form similar to Eq. (C.2), then it can be shown that

$$\left[\frac{1}{2}\mathcal{A}, \frac{1}{2}\mathcal{B}\right] = \frac{1}{2}\mathcal{C}\,, \tag{C.20}$$

where

$$\mathcal{C} = \mathbf{a}^{\dagger}Z\,[ZA, ZB]\,\mathbf{a}\,.$$

Using the Baker-Campbell-Hausdorff we can get our final expression as

$$\left[\mathrm{Tr}\left(e^{\hat{A}}e^{\hat{B}}\right)\right]^2 = \det(Z)e^{-\mathrm{tr}(A^{(0)}+B^{(0)})}\det(1-e^{ZA}e^{ZB})^{-1}\,. \tag{C.21}$$

D Correlation matrix from Klich's determinant formula

This section gives the expressions used to calculate the equal time correlation matrix after the quench $F_>(t,t)$, using the formulas developed in the last section. Before we give the general expressions, first let us note a result that will be used in the rest of the section

$$\begin{aligned}\lim_{\beta\to\infty}\left[\frac{\mathrm{Tr}\left(e^{\hat{A}}e^{-\beta\mathcal{H}_<}\right)}{\mathrm{Tr}\left(e^{-\beta\mathcal{H}_<}\right)}\right]^2 &= \lim_{\beta\to\infty} e^{-\mathrm{tr}A^{(0)}}\frac{\det(1-e^{ZA}e^{-\beta ZH_<})^{-1}}{\det(1-e^{-\beta ZH_<})^{-1}}\\ &= \lim_{\beta\to\infty} e^{-\mathrm{tr}A^{(0)}}\det\left(\frac{1}{1-e^{-\beta\Lambda_<}}-Q^{-1}e^{ZA}Q\frac{e^{-\beta\Lambda_<}}{1-e^{-\beta\Lambda_<}}\right)^{-1}\\ &= e^{-\mathrm{tr}A^{(0)}}\det\left(\frac{\mathbb{I}_{2J}+Z}{2}+Q^{-1}e^{ZA}Q\frac{\mathbb{I}_{2J}-Z}{2}\right)^{-1},\end{aligned} \tag{D.1}$$

where the diagonal matrix $\Lambda_<$ of dimensions $2J$ has positive eigenvalues in the first half on the diagonal and negative eigenvalues in the second half.

Now let us write down the expressions for elements of the correlation matrix

$$\begin{aligned}F_{>,ij}(t,t)=\left\langle \mathbf{a}^\dagger(t)_i\mathbf{a}(t)_j\right\rangle &= \partial_\chi\left\langle e^{\chi\mathbf{a}^\dagger(t)_i\mathbf{a}(t)_j}\right\rangle_{\chi=0}\\ &\approx \lim_{\delta\chi\to0}\frac{\left\langle e^{\delta\chi\mathbf{a}^\dagger(t)_i\mathbf{a}(t)_j}\right\rangle-1}{\delta\chi}\\ &= \lim_{\delta\chi\to0}\frac{\sqrt{\left\langle e^{\delta\chi\mathbf{a}^\dagger(t)_i\mathbf{a}(t)_j}\right\rangle^2}-1}{\delta\chi}\\ &= \lim_{\delta\chi\to0}\frac{\sqrt{\lim_{\beta\to\infty}\frac{\mathrm{Tr}\left(e^{i\mathcal{H}_>t}e^{\hat{\chi}}e^{-i\mathcal{H}_>t}e^{-\beta\mathcal{H}_<}\right)^2}{\mathrm{Tr}\left(e^{-\beta\mathcal{H}_<}\right)^2}}-1}{\delta\chi},\end{aligned} \tag{D.2}$$

where we have defined the operator $\hat{\chi}$ as follows

$$\begin{aligned}\hat{\chi}&=\delta\chi\left(\frac{1}{2}\mathbf{a}^\dagger M\mathbf{a}\pm\frac{1}{2}\mathrm{tr}M^{(0)}\right),\\ M&=\begin{pmatrix}M^{(0)} & M^{(1)}\\ M^{(2)} & \left(M^{(0)}\right)^T\end{pmatrix},\end{aligned} \tag{D.3}$$

such that

$$\begin{aligned}M^{(1)}&=\left(M^{(1)}\right)^T,\\ M^{(2)}&=\left(M^{(2)}\right)^T.\end{aligned}$$

The elements of the matrix M and the plus or minus sign in the definition of $\hat{\chi}$ depend on the value of the indices i and j.

$$\begin{aligned}F_{>,ij}(t,t)&=\lim_{\delta\chi\to0}\frac{\sqrt{\lim_{\beta\to\infty}\frac{\mathrm{Tr}\left(e^{i\mathcal{H}_>t}e^{\hat{\chi}}e^{-i\mathcal{H}_>t}e^{-\beta\mathcal{H}_<}\right)^2}{\mathrm{Tr}\left(e^{-\beta\mathcal{H}_<}\right)^2}}-1}{\delta\chi}\\ &=\lim_{\delta\chi\to0}\frac{\sqrt{\lim_{\beta\to\infty}\frac{e^{\pm\delta\chi\mathrm{tr}M^{(0)}}\det\left(1-e^{iZ_{2J}H_>t}e^{\delta\chi Z_{2J}M}e^{-iZ_{2J}H_>t}e^{-\beta Z_{2J}H_<}\right)^{-1}}{\det\left(1-e^{-\beta Z_{2J}H_<}\right)^{-1}}}-1}{\delta\chi},\end{aligned} \tag{D.4}$$

where we have used Eq. (C.21). Expanding the exponentials upto first order in $\delta\chi$, and using the identity $\det(\mathbb{I}+\epsilon A)\approx 1+\epsilon\,\mathrm{tr}(A)+\mathcal{O}(\epsilon^2)$, we get

$$F_{>,ij}(t,t)=\lim_{\delta\chi\to 0}\frac{e^{\pm\delta\chi\,\mathrm{tr}\frac{M^{(0)}}{2}}\left(1+\frac{\delta\chi}{2}\mathrm{tr}\left[Q^{-1}e^{iZH_{>}t}ZMe^{-iZH_{>}t}Q(\mathbb{I}_{2J}-Z)\right]\right)^{-1/2}-1}{\delta\chi}. \tag{D.5}$$

If $\mathrm{tr}M^{(0)}=0$

$$\begin{aligned}F_{>,ij}(t,t)&=\lim_{\delta\chi\to 0}\frac{\left(1+\frac{\delta\chi}{2}\mathrm{tr}\left[Q^{-1}e^{iZH_{>}t}ZMe^{-iZH_{>}t}Q(\mathbb{I}_{2J}-Z)\right]\right)^{-1/2}-1}{\delta\chi}\\&\approx\lim_{\delta\chi\to 0}\frac{1-\frac{\delta\chi}{4}\mathrm{tr}\left[Q^{-1}e^{iZH_{>}t}ZMe^{-iZH_{>}t}Q(\mathbb{I}_{2J}-Z)\right]-1}{\delta\chi}\\&=-\frac{\mathrm{tr}\left[Q^{-1}e^{iZH_{>}t}ZMe^{-iZH_{>}t}Q(\mathbb{I}_{2J}-Z)\right]}{4},\end{aligned} \tag{D.6}$$

instead if $\mathrm{tr}M^{(0)}=1$ with a negative sign in the definition of $\hat{\chi}$

$$\begin{aligned}F_{>,ij}(t,t)&=\lim_{\delta\chi\to 0}\frac{e^{-\frac{\delta\chi}{2}}\left(1+\frac{\delta\chi}{2}\mathrm{tr}\left[Q^{-1}e^{iZH_{>}t}ZMe^{-iZH_{>}t}Q(\mathbb{I}_{2J}-Z)\right]\right)^{-1/2}-1}{\delta\chi}\\&\approx\lim_{\delta\chi\to 0}\frac{e^{-\frac{\delta\chi}{2}}-e^{-\frac{\delta\chi}{2}}\frac{\delta\chi}{4}\mathrm{tr}\left[Q^{-1}e^{iZH_{>}t}ZMe^{-iZH_{>}t}Q(\mathbb{I}_{2J}-Z)\right]-1}{\delta\chi}\\&=-\frac{1}{2}-\frac{\mathrm{tr}\left[Q^{-1}e^{iZH_{>}t}ZMe^{-iZH_{>}t}Q(\mathbb{I}_{2J}-Z)\right]}{4},\end{aligned} \tag{D.7}$$

and finally if $\mathrm{tr}M^{(0)}=1$ with a plus sign in the definition of $\hat{\chi}$

$$\begin{aligned}F_{>,ij}(t,t)&=\lim_{\delta\chi\to 0}\frac{e^{\frac{\delta\chi}{2}}\left(1+\frac{\delta\chi}{2}\mathrm{tr}\left[Q^{-1}e^{iZH_{>}t}ZMe^{-iZH_{>}t}Q(\mathbb{I}_{2J}-Z)\right]\right)^{-1/2}-1}{\delta\chi}\\&\approx\lim_{\delta\chi\to 0}\frac{e^{\frac{\delta\chi}{2}}-e^{\frac{\delta\chi}{2}}\frac{\delta\chi}{4}\mathrm{tr}\left[Q^{-1}e^{iZH_{>}t}ZMe^{-iZH_{>}t}Q(\mathbb{I}_{2J}-Z)\right]-1}{\delta\chi}\\&=\frac{1}{2}-\frac{\mathrm{tr}\left[Q^{-1}e^{iZH_{>}t}ZMe^{-iZH_{>}t}Q(\mathbb{I}_{2J}-Z)\right]}{4}.\end{aligned} \tag{D.8}$$

The matrix M and the operator $\hat{\chi}$ will have the following forms depending on the indices i and j.

- $i\le J, j\le J$:

  The matrices $M^{(1)}$ and $M^{(2)}$ will only contain zeros, and

$$\begin{aligned}M^{(0)}_{lk}&=\begin{cases}0, & l\neq i,\ k\neq j,\\ 1, & l=i,\ k=j,\end{cases}\\\hat{\chi}&=\delta\chi\left(\frac{1}{2}\mathbf{a}^{\dagger}M\mathbf{a}-\frac{1}{2}\mathrm{tr}M^{(0)}\right),\end{aligned} \tag{D.9}$$

  the indices l and k run from 1 to J. Here, $\mathrm{tr}M^{(0)}=1$ only if $i=j$ otherwise it's zero.

- $i \leq J, j > J$:

  The matrices $M^{(0)}$ and $M^{(2)}$ will only contain zeros, and

$$M^{(1)}_{lk} = \begin{cases} 1, & l = j-J,\ k = i, \\ 1, & l = i,\ k = j-J, \\ 0, & \text{every other element}, \end{cases} \qquad \hat{\chi} = \delta\chi \frac{1}{2}\mathbf{a}^\dagger M \mathbf{a}. \tag{D.10}$$

  Here, $\mathrm{tr}M^{(0)}$ is always zero.

- $i > J, j \leq J$:

  The matrices $M^{(0)}$ and $M^{(1)}$ will only contain zeros, and

$$M^{(2)}_{lk} = \begin{cases} 1, & l = j,\ k = i-J, \\ 1, & l = i-J,\ k = j, \\ 0, & \text{every other element}, \end{cases} \qquad \hat{\chi} = \delta\chi \frac{1}{2}\mathbf{a}^\dagger M \mathbf{a}. \tag{D.11}$$

  Again, $\mathrm{tr}M^{(0)}$ is always zero.

- $i > J, j > J$:

  The matrices $M^{(1)}$ and $M^{(2)}$ will only contain zeros, and

$$M^{(0)}_{lk} = \begin{cases} 0, & l \neq i-J,\ k \neq j-J, \\ 1, & l = i-J,\ k = j-J, \end{cases} \qquad \hat{\chi} = \delta\chi \left(\frac{1}{2}\mathbf{a}^\dagger M \mathbf{a} + \frac{1}{2}\mathrm{tr}M^{(0)}\right). \tag{D.12}$$

  Here, $\mathrm{tr}M^{(0)} = 1$ only if $i = j$ otherwise it's zero.

E Hawking-Unruh radiation on a lattice

In this appendix we argue that the Hawking radiation can indeed be obtained on a lattice if the change in the parameters of the system, equivalently the change in metric, is smooth enough (with some restrictions). However as also pointed out in the main text, there will be essential differences between continuum and lattice models. To begin let us consider the following Lagrangian

$$\mathcal{L} = \int dx \left(\frac{1}{2u}\dot{\phi}^2 - \frac{v(x)}{u}\dot{\phi}\partial_x\phi + \frac{v^2(x)-u^2}{2u}(\partial_x\phi)^2\right). \tag{E.1}$$

This form of Lagrangian is what most works on analogue horizons try to emulate [43]. An important aspect of this field theory is that the determinant of the metric remains constant. This is in contrast to our proposal, where we only modulate the inductance as a function of position, which does not conserve the determinant of the metric in the continuum limit. But our goal here is to compare the result of lattice realisations and continuum realisations, where we choose to consider the simplest possible case with constant determinant.

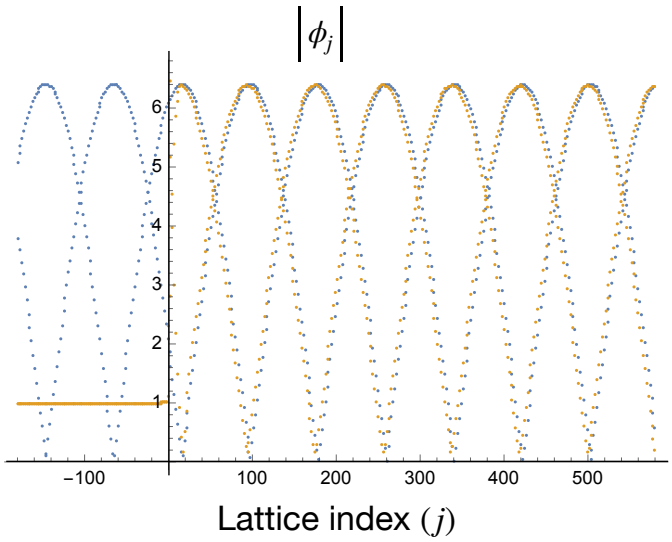

Figure 9: In this figure we have plotted the absolute value of ϕ_j as a function of j. Since the incoming mode was chosen to be a plane wave therefore we see $|\phi_j| = 1$ for $j < -J$. The transmitted mode (orange dotted lines), obtained numerically, shows a beating pattern. To confirm that the beating pattern is produced by a wave vector near $\widetilde{k} = 0$ and the other one near $\widetilde{k} = \pi$, we have also plotted a function $A\left(e^{i\widetilde{k}\Delta x j} + e^{i(\pi-\widetilde{k}\Delta x)j)}\right)$ on the same figure. We see that the theoretical and numerical transmitted modes agree with each other if we scale the theoretical one appropriately using the constant A.

Now we set this field theory on a one dimensional infinite lattice. The discretised version of the Lagrangian is

$$\mathcal{L} = \frac{\Delta x}{u}\sum_j \dot{\phi}_j^2 - \sum_j \frac{v_j}{u}\dot{\phi}_j\left(\phi_{j+1}-\phi_{j-1}\right) - \sum_j \frac{u^2-v_j^2}{4u\Delta x}\left(\phi_{j+1}-\phi_{j-1}\right)^2 . \tag{E.2}$$

Note that we consider next-to-nearest neighbour coupling in order to avoid any issues due to instabilities unrelated to the horizon (see also main text). Therefore, in this model the lattice constant is best defined as $2\Delta x$. The conjugate field is

$$\pi_j = \frac{1}{2\Delta x}\frac{\partial \mathcal{L}}{\partial \dot{\phi}_j} = \frac{1}{u}\dot{\phi}_j - \frac{v_j}{2u\Delta x}\left(\phi_{j+1}-\phi_{j-1}\right) . \tag{E.3}$$

Using the Legendre transform we can write the Hamiltonian

$$\mathcal{H} = 2\Delta x\frac{u}{2}\sum_j \pi_j^2 + \frac{v_j}{2}\sum_j\left\{\pi_j,\left(\phi_{j+1}-\phi_{j-1}\right)\right\} + \sum_j \frac{u}{4\Delta x}\left(\phi_{j+1}-\phi_{j-1}\right)^2 . \tag{E.4}$$

Now the equations of motion will be

$$\begin{aligned} 2\Delta x\ddot{\phi}_j = {} & v_{j+1}\dot{\phi}_{j+1} - v_{j-1}\dot{\phi}_{j-1} + v_j\left(\dot{\phi}_{j+1}-\dot{\phi}_{j-1}\right) \\ & - \frac{u^2-v_{j-1}^2}{2\Delta x}\left(\phi_j-\phi_{j-2}\right) - \frac{u^2-v_{j+1}^2}{2\Delta x}\left(\phi_j-\phi_{j+2}\right) . \end{aligned} \tag{E.5}$$

For the translationally invariant case ($v_j = v$) this reduces to

$$2\Delta x\ddot{\phi}_j = 2v\left(\dot{\phi}_{j+1}-\dot{\phi}_{j-1}\right) - \frac{u^2-v^2}{2\Delta x}\left(2\phi_j-\phi_{j-2}-\phi_{j+2}\right) . \tag{E.6}$$

Using the following ansatz $\phi_j(t) = e^{i\omega t}e^{ik\Delta x j}$, we get the dispersion relation

$$\omega_\pm(k) = v\frac{\sin(k\Delta x)}{\Delta x} \pm u\left|\frac{\sin(k\Delta x)}{\Delta x}\right|. \tag{E.7}$$

In the limit $\Delta x \to 0$, this yields the same dispersion relation as in the continuum case. Additionally, in this dispersion relation the sector near $k = 0$ and $k = \pi$ mirror each other which is reminiscent of the dispersion relation in Eq. (18).

We now come to the inhomogeneous system. Since the Lagrangian is time-independent we can still write the ansatz $\phi_j(t) = e^{i\omega t}\phi_j$, which gives us the following recurrence relation

$$\begin{aligned}-\omega^2\frac{2\Delta x}{u}\phi_j = i\omega\frac{v_{j+1}}{u}\phi_{j+1} - i\omega\frac{v_{j-1}}{u}\phi_{j-1} + i\omega\frac{v_j}{u}\left(\phi_{j+1}-\phi_{j-1}\right)\\ -\frac{u^2-v_{j-1}^2}{2u\Delta x}\left(\phi_j-\phi_{j-2}\right) - \frac{u^2-v_{j+1}^2}{2u\Delta x}\left(\phi_j-\phi_{j+2}\right),\end{aligned} \tag{E.8}$$

which we can re-write as

$$\begin{aligned}\phi_{j+2} = \phi_j - \frac{4\omega^2\Delta x^2}{u^2-v_{j+1}^2}\phi_j + \frac{2i\omega\Delta x}{u^2-v_{j+1}^2}\left(v_{j-1}\phi_{j-1} - v_{j+1}\phi_{j+1}\right)\\ -\frac{2i\omega\Delta x}{u^2-v_{j+1}^2}v_j\left(\phi_{j+1}-\phi_{j-1}\right) + \frac{u^2-v_{j-1}^2}{u^2-v_{j+1}^2}\left(\phi_j-\phi_{j-2}\right).\end{aligned} \tag{E.9}$$

We are interested in the solution to this recurrence relation for the following profile

$$v_j = \begin{cases} v_0, & j \to -\infty, \\ v_1, & j \to \infty, \end{cases} \tag{E.10}$$

such that $v_0 < u < v_1$. With this profile of the parameter v_j, in the asymptotically left region the signals will move in both left and right directions while in asymptotically right region the signals will only move towards right, and somewhere in the boundary between these two region for some j' we will have $v_{j'} \le u < v_{j'+1}$, this is the event horizon.

In general, solving the recurrence relation in Eq. (E.9) for an arbitrary profile of v_j is not analytically possible, therefore we will tackle this problem numerically. We use a linear profile for the parameter v_j (for a smooth horizon, we can always approximate the change in its neighbourhood as linear) such that

$$v_j = \begin{cases} 0, & j < -J, \\ v_{\max}\frac{j+J}{2J}, & -J \le j \le J, \\ v_{\max}, & j > J, \end{cases} \tag{E.11}$$

where $v_{\max} = \frac{2u}{1-\frac{\alpha}{J}}$ and α (with $0 < \alpha < 1$, hence $\alpha \ll J$) is a real number that decides a particular detail of the discretisation of v_j with respect to u. For example, if $\alpha = 0$ then $v_{j=0} = u$, or if $\alpha = 0.5$ then u will lie exactly in middle of $v_{j'}$ and $v_{j'+1}$. That is, α controls whether the profile v_j actually "hits" the velocity u or not. In fact, for $\alpha = 0, 1$, the problem is ill-defined as the above recurrence relation contains singularities. For a well-defined answer, the parameter α should lie between 0 and 1 (as specified above).

To construct scattering modes for the Hamiltonian we start with the following incoming plane wave

$$\phi_{\text{in}} = \sum_{j<-J} e^{ik\Delta x j}, \quad 0 < k\Delta x \ll 1, \tag{E.12}$$

in the region with $v_j = 0$ and energy $\omega_+(k) = u \sin(k\Delta x)/\Delta x$. Using the recurrence relation we obtain the transmitted mode as shown in Fig. 9, from this we conclude that the scattering modes with positive energy are of the form

$$\phi_k = \sum_{j<-J} e^{ik\Delta x j} + C(\omega_{k,+}) \sum_{j\geq -J} \left(e^{i\tilde{k}\Delta x j} + e^{i(\pi-\tilde{k}\Delta x)j} \right), \tag{E.13}$$

where

$$\tilde{k} = \frac{1}{\Delta x} \arcsin \frac{\omega_{k,+}\Delta x}{v_{\max} - u}, \tag{E.14}$$

is obtained by energy matching and $C(\omega_{k,+})$ is a constant depending on the energy of the incoming wave. We find that $C(\omega_{k,+})$ takes the following form

$$C(\omega_{k,+}) = \gamma e^{\frac{\pi}{a}\omega_{k,+}}, \tag{E.15}$$

with fitting parameters γ and a. Here, the factor γ depends on the exact details of the discretisation of v_j, if $\alpha = 0.5$ and therefore u lies exactly in the middle of some $v_{j'}$ and $v_{j'+1}$ then $\gamma = 0.5$ (see Fig. 10). As we change α and therefore the asymmetry of u with respect to $v_{j'}$ and $v_{j'+1}$, the value of γ diverges as we approach the singular case $\alpha = 0$. This can also be seen from the recurrence relation in Eq. (E.9), where if some $v_j = u$, the equation becomes non-analytic. The factor $e^{\pi\omega_{k,+}/a}$ is the expected Hawking factor where a is the analogue surface gravity. Indeed, from Fig. 11 we can see that it is given by the derivative of the group velocity across the horizon,

$$a = \frac{v_{\max}}{2J\Delta x}, \tag{E.16}$$

i.e., it is the discrete derivative of the group velocity. Another important feature we can gleam from Eq. (E.13) is that the incoming mode scatters into two different modes with same energy, but with different wave vector: one near $\tilde{k} = 0$ and another near $\tilde{k} = \pi$. This in turn implies that even for the case of smooth variation of parameters, in a lattice model, the ambiguity between black/white hole nature of the horizon still remains.

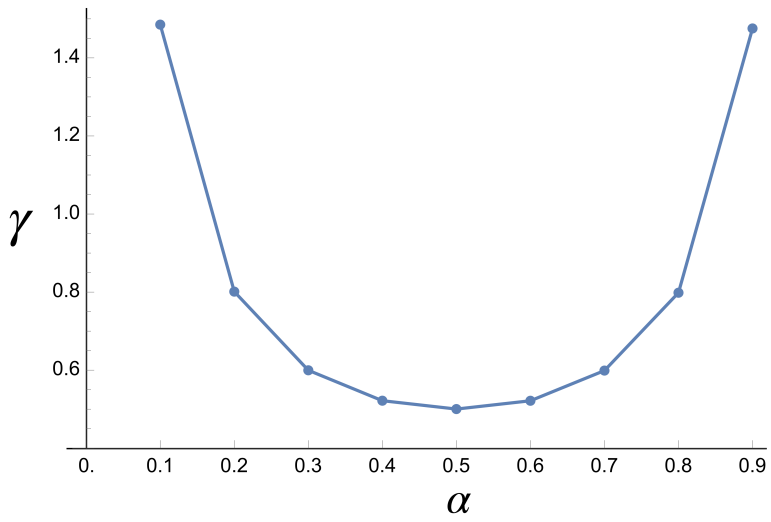

Figure 10: In this figure we have plotted γ from Eq. (E.15) against α, hence confirming that $C(\omega_{k,+})$ depends on the details of discretisation of the lattice.

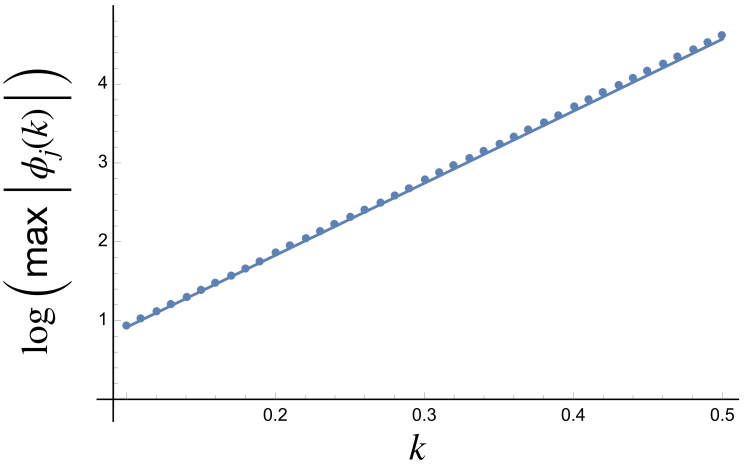

Figure 11: In this figure we have plotted the logarithm of the maximum of $|\phi_j(k)|$ against k (the wave vector of the incoming mode) for $\alpha = 0.5$. To confirm that our theoretical prediction of the surface gravity $a = v_{\max}/2J\Delta x$ matches the numerical calculation. The dotted line is extracted from the numerical calculation and the smooth line is plotted using the analytical expression in Eq. (E.16). Also note that for other values of α we get the same slope i.e. the same surface gravity but different intercept i.e. different γ.

F Effect of disorder

In this appendix we briefly discuss the effect of disorder in the circuit parameters on the evaporation of the horizons. We achieve this by independently introducing disorder in the gyrator term G and the inductive term E_L, the disorder in both the terms is taken to be normally distributed, hence at each lattice site the value of the gyrator conductance G and the inductance is drawn from the following probability distributions

$$\begin{aligned}\rho(G) &= \frac{1}{\sqrt{2\pi\sigma_G^2}} e^{-\frac{(G-G_0)^2}{2\sigma_G^2}}, \\ \rho(E_L) &= \frac{1}{\sqrt{2\pi\sigma_{E_L}^2}} e^{-\frac{(E_L-E_{L0})^2}{2\sigma_{E_L}^2}}.\end{aligned} \tag{F.1}$$

Here, G_0 and E_{L0} are the mean of the normal distributions corresponding to gyrator conductance and inductance respectively. Their values are equal to the respective values of these parameters in Sec. (5), and the standard deviations σ_G and σ_{E_L} encode the strength of disorder. The quench is performed by flipping the value of inductances in the region $30 \leq j \leq 70$ to negative, same as in the main text. Additionally, we will only look at the correlations of phase differences in both the circuits, but not at the correlations of conjugate charge as they do not provide any new insight on the effect of disorder.

For the circuit with only nearest neighbour connections (Figs. (12) and (13)) we can see that for small disorder, i.e. $\sigma_G/G_0, \sigma_{E_L}/E_{L0} \leq 5\%$ (the upper row in both the images), there is not much difference in the time evolution of quantum fluctuations compared to the case of no disorder (Fig. (6a)). For larger disorder (the lower row) the behaviour of correlations in the wormhole region does differ from the circuit with no disorder, however the effect on the evaporation of the black hole horizon still seems to be negligible. Furthermore for disorder of similar relative strength, the disorder in gyrators is more impactful than the disorder in inductors. For the circuit where JJs connect next nearest neighbours (Figs. (14) and (15)) already

for small disorder (again the upper row in both the images), the time evolution of quantum fluctuations in the wormhole region is different from the case of no disorder (Fig. (7a)), but the effect of disorder on evaporation of the horizons is negligible. For larger disorder (the lower row) both the behaviour of correlations in the wormhole region, and the evaporation of the horizons is significantly affected. Also, again we see that for disorder of similar relative strength, the disorder in gyrators is more impactful than the disorder in inductors.

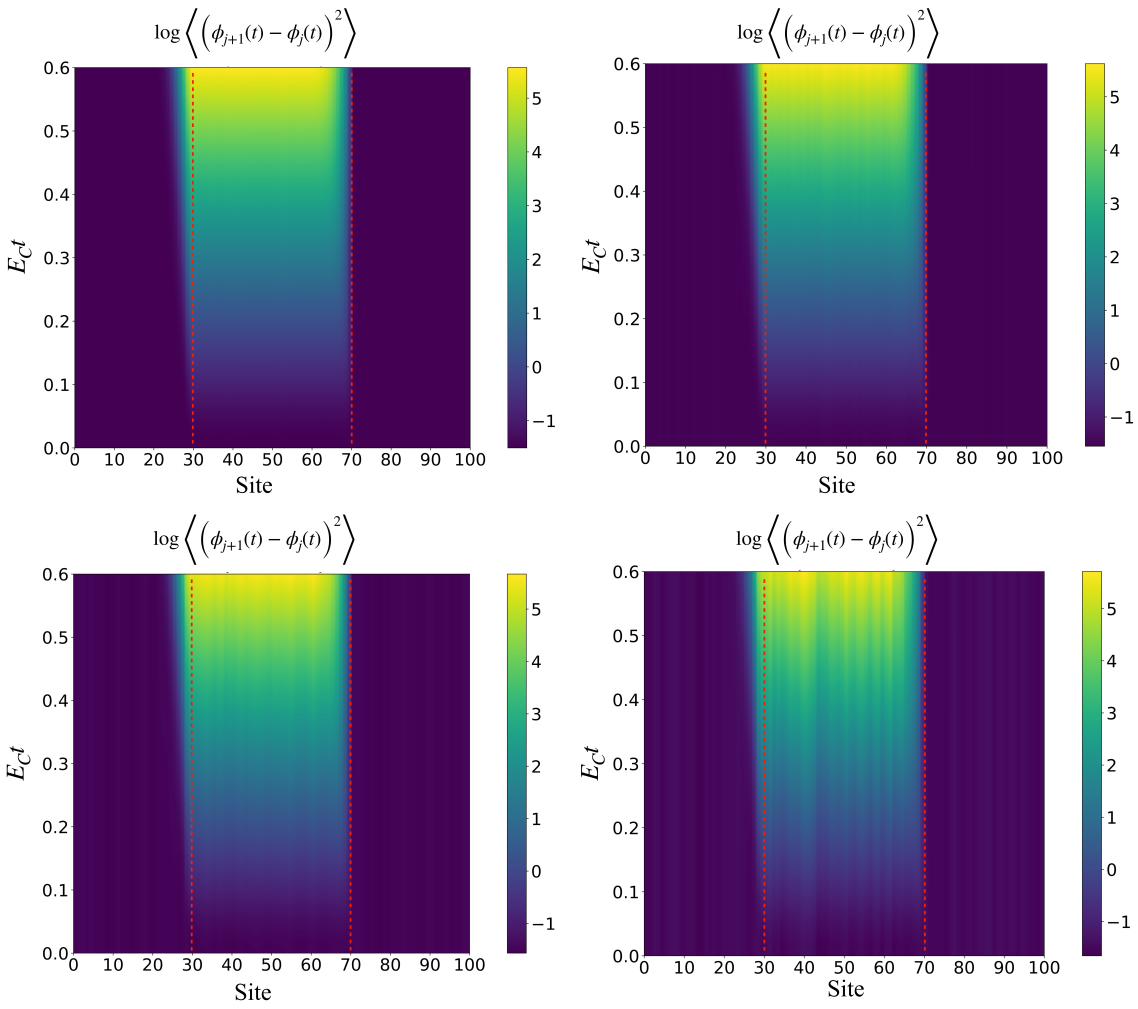

Figure 12: The four figures above show the time evolution of the quantum fluctuations of the phase difference in a circuit with Josephson junctions connecting the nearest neighbours and with disorder in G. Starting with the upper left figure, and moving in a Z pattern the relative strength of disorder goes as $\sigma_G/G_0 \sim 1\%, 5\%, 10\%, 20\%$.

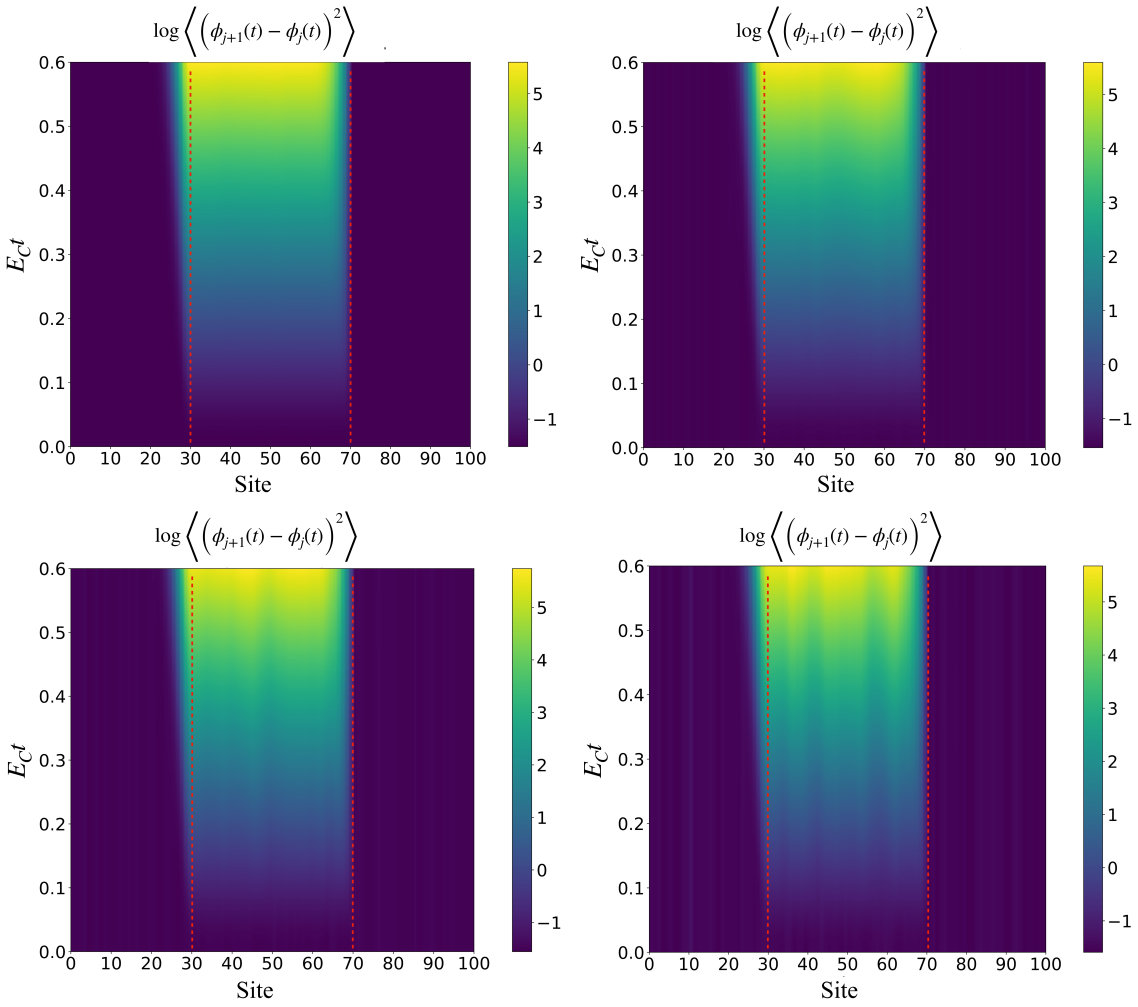

Figure 13: The four figures above show the time evolution of the quantum fluctuations of the phase difference in a circuit with Josephson junctions connecting the nearest neighbours and with disorder in E_L. Starting with the upper left figure, and moving in a Z pattern the strength of disorder goes as $\sigma_{E_L}/E_{L0} \sim 1\%, 5\%, 10\%, 20\%$.

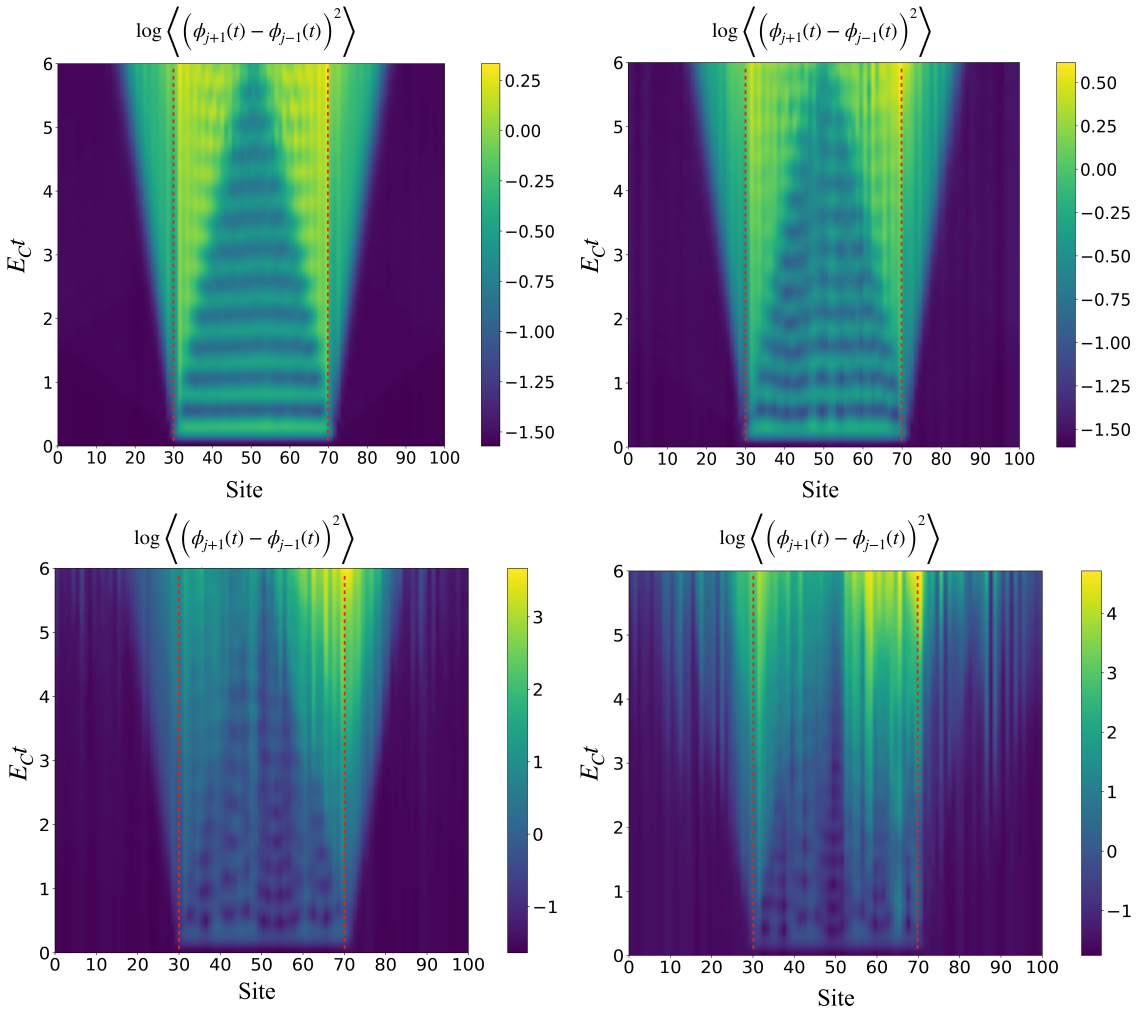

Figure 14: The four figures above show the time evolution of the quantum fluctuations of the phase difference in a circuit with Josephson junctions connecting the next nearest neighbours and with disorder in G. Starting with the upper left figure, and moving in a Z pattern the strength of disorder goes as $\sigma_G/G_0 \sim 1\%, 5\%, 10\%, 20\%$.

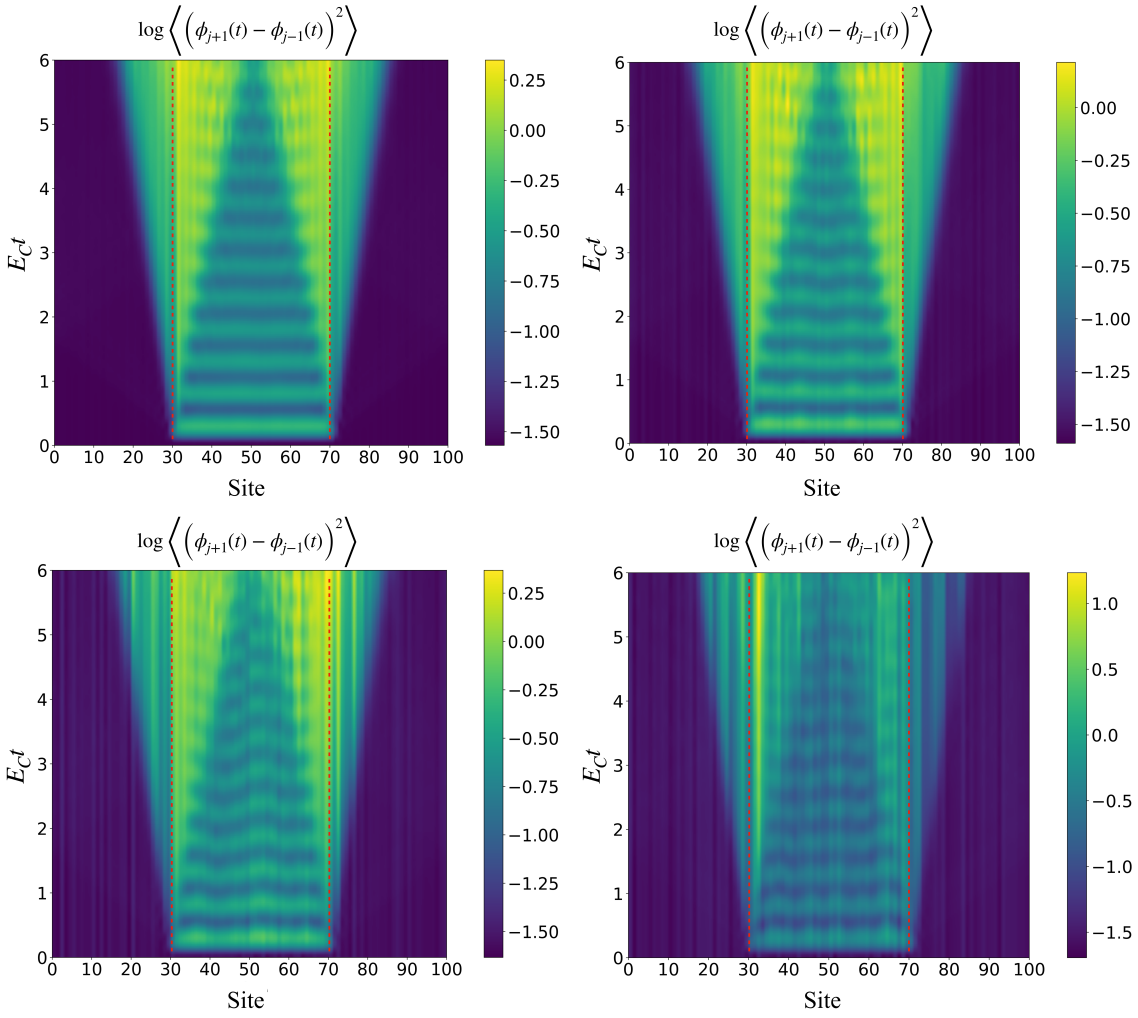

Figure 15: The four figures above show the time evolution of the quantum fluctuations of the phase difference in a circuit with Josephson junctions connecting the next nearest neighbours and with disorder in E_L. Starting with the upper left figure, and moving in a Z pattern the strength of disorder goes as $\sigma_{E_L}/E_{L0} \sim 1\%, 5\%, 10\%, 20\%$.

References

[1] G. 't Hooft and M. Veltman, *One-loop divergencies in the theory of gravitation*, in *Euclidean quantum gravity*, World Scientific, Singapore, ISBN 9789810205157 (1993), doi:10.1142/9789814539395_0001.

[2] M. H. Goroff and A. Sagnotti, *The ultraviolet behavior of Einstein gravity*, Nucl. Phys. B **266**, 709 (1986), doi:10.1016/0550-3213(86)90193-8.

[3] R. Penrose, *On the gravitization of quantum mechanics 1: Quantum state reduction*, Found. Phys. **44**, 557 (2014), doi:10.1007/s10701-013-9770-0.

[4] J. K. Hoskins, R. D. Newman, R. Spero and J. Schultz, *Experimental tests of the gravitational inverse-square law for mass separations from 2 to 105 cm*, Phys. Rev. D **32**, 3084 (1985), doi:10.1103/PhysRevD.32.3084.

[5] V. Mitrofanov and O. Ponomareva, *Experimental test of gravitation at small distances*, Sov. J. Exp. Theor. Phys. **67**, 1963 (1988).

[6] J. G. Lee, E. G. Adelberger, T. S. Cook, S. M. Fleischer and B. R. Heckel, *New test of the gravitational $1/r^2$ law at separations down to 52 μm*, Phys. Rev. Lett. **124**, 101101 (2020), doi:10.1103/PhysRevLett.124.101101 [preprint doi:10.48550/arXiv.2002.11761].

[7] T. Westphal, H. Hepach, J. Pfaff and M. Aspelmeyer, *Measurement of gravitational coupling between millimetre-sized masses*, Nature **591**, 225 (2021), doi:10.1038/s41586-021-03250-7.

[8] S. Gerlich, S. Eibenberger, M. Tomandl, S. Nimmrichter, K. Hornberger, P. J. Fagan, J. Tüxen, M. Mayor and M. Arndt, *Quantum interference of large organic molecules*, Nat. Commun. **2**, 263 (2011), doi:10.1038/ncomms1263.

[9] S. Eibenberger, S. Gerlich, M. Arndt, M. Mayor and J. Tüxen, *Matter–wave interference of particles selected from a molecular library with masses exceeding 10000 amu*, Phys. Chem. Chem. Phys. **15**, 14696 (2013), doi:10.1039/C3CP51500A [preprint doi:10.48550/arXiv.1310.8343].

[10] O. Romero-Isart, *Coherent inflation for large quantum superpositions of levitated microspheres*, New J. Phys. **19**, 123029 (2017), doi:10.1088/1367-2630/aa99bf [preprint doi:10.48550/arXiv.1612.04290].

[11] H. Pino, J. Prat-Camps, K. Sinha, B. P. Venkatesh and O. Romero-Isart, *On-chip quantum interference of a superconducting microsphere*, Quantum Sci. Technol. **3**, 025001 (2018), doi:10.1088/2058-9565/aa9d15 [preprint doi:10.48550/arXiv.1603.01553].

[12] Y. Y. Fein, P. Geyer, P. Zwick, F. Kiałka, S. Pedalino, M. Mayor, S. Gerlich and M. Arndt, *Quantum superposition of molecules beyond 25 kDa*, Nat. Phys. **15**, 1242 (2019), doi:10.1038/s41567-019-0663-9.

[13] U. Delić, M. Reisenbauer, K. Dare, D. Grass, V. Vuletić, N. Kiesel and M. Aspelmeyer, *Cooling of a levitated nanoparticle to the motional quantum ground state*, Science **367**, 892 (2020), doi:10.1126/science.aba3993 [preprint doi:10.48550/arXiv.1911.04406].

[14] F. Tebbenjohanns, M. L. Mattana, M. Rossi, M. Frimmer and L. Novotny, *Quantum control of a nanoparticle optically levitated in cryogenic free space*, Nature **595**, 378 (2021), doi:10.1038/s41586-021-03617-w [preprint doi:10.48550/arXiv.2103.03853].

[15] C. Barceló, S. Liberati and M. Visser, *Analogue gravity*, Living Rev. Relativ. **14**, 3 (2011), doi:10.12942/lrr-2011-3.

[16] S. Sachdev and J. Ye, *Gapless spin-fluid ground state in a random quantum Heisenberg magnet*, Phys. Rev. Lett. **70**, 3339 (1993), doi:10.1103/PhysRevLett.70.3339 [preprint doi:10.48550/arXiv.cond-mat/9212030].

[17] S. Sachdev, *Bekenstein-Hawking entropy and strange metals*, Phys. Rev. X **5**, 041025 (2015), doi:10.1103/PhysRevX.5.041025 [preprint doi:10.48550/arXiv.1506.05111].

[18] D. Bagrets, A. Altland and A. Kamenev, *Sachdev–Ye–Kitaev model as Liouville quantum mechanics*, Nucl. Phys. B **911**, 191 (2016), doi:10.1016/j.nuclphysb.2016.08.002 [preprint doi:10.48550/arXiv.1607.00694].

[19] A. Kitaev and S. J. Suh, *The soft mode in the Sachdev-Ye-Kitaev model and its gravity dual*, J. High Energy Phys. **05**, 183 (2018), doi:10.1007/JHEP05(2018)183.

[20] A. Kitaev and S. J. Suh, *Statistical mechanics of a two-dimensional black hole*, J. High Energy Phys. **05**, 198 (2019), doi:10.1007/JHEP05(2019)198.

[21] D. Jafferis, A. Zlokapa, J. D. Lykken, D. K. Kolchmeyer, S. I. Davis, N. Lauk, H. Neven and M. Spiropulu, *Traversable wormhole dynamics on a quantum processor*, Nature **612**, 51 (2022), doi:10.1038/s41586-022-05424-3.

[22] C. Barceló, S. Liberati and M. Visser, *Probing semiclassical analogue gravity in Bose-Einstein condensates with widely tunable interactions*, Phys. Rev. A **68**, 053613 (2003), doi:10.1103/PhysRevA.68.053613 [preprint doi:10.48550/arXiv.cond-mat/0307491].

[23] P. O. Fedichev and U. R. Fischer, *"Cosmological" quasiparticle production in harmonically trapped superfluid gases*, Phys. Rev. A **69**, 033602 (2004), doi:10.1103/PhysRevA.69.033602 [preprint doi:10.48550/arXiv.cond-mat/0303063].

[24] U. Fischer and R. Schützhold, *Quantum simulation of cosmic inflation in two-component Bose-Einstein condensates*, Phys. Rev. A **70**, 063615 (2004), doi:10.1103/PhysRevA.70.063615 [preprint doi:10.48550/arXiv.cond-mat/0406470].

[25] P. Jain, S. Weinfurtner, M. Visser and C. W. Gardiner, *Analogue model of a Friedmann-Robertson-Walker universe in Bose-Einstein condensates: Application of the classical field method*, Phys. Rev. A **76**, 033616 (2007), doi:10.1103/PhysRevA.76.033616 [preprint doi:10.48550/arXiv.0705.2077].

[26] A. Prain, S. Fagnocchi and S. Liberati, *Analogue cosmological particle creation: Quantum correlations in expanding Bose-Einstein condensates*, Phys. Rev. D **82**, 105018 (2010), doi:10.1103/PhysRevD.82.105018 [preprint doi:10.48550/arXiv.1009.0647].

[27] J. Steinhauer, M. Abuzarli, T. Aladjidi, T. Bienaimé, C. Piekarski, W. Liu, E. Giacobino, A. Bramati and Q. Glorieux, *Analogue cosmological particle creation in an ultracold quantum fluid of light*, Nat. Commun. **13**, 2890 (2022), doi:10.1038/s41467-022-30603-1 [preprint doi:10.48550/arXiv.2102.08279].

[28] W. G. Unruh, *Experimental black-hole evaporation?*, Phys. Rev. Lett. **46**, 1351 (1981), doi:10.1103/PhysRevLett.46.1351.

[29] Y. Kedem, E. J. Bergholtz and F. Wilczek, *Black and white holes at material junctions*, Phys. Rev. Res. **2**, 043285 (2020), doi:10.1103/PhysRevResearch.2.043285 [preprint doi:10.48550/arXiv.2001.02625].

[30] R. P. Schmit, B. G. Taketani and F. K. Wilhelm, *Quantum simulation of particle creation in curved space-time*, PLOS One **15**, e0229382 (2020), doi:10.1371/journal.pone.0229382 [preprint doi:10.48550/arXiv.1804.04092].

[31] C. De Beule, S. Groenendijk, T. Meng and T. Schmidt, *Artificial event horizons in Weyl semimetal heterostructures and their non-equilibrium signatures*, SciPost Phys. **11**, 095 (2021), doi:10.21468/SciPostPhys.11.5.095 [preprint doi:10.48550/arXiv.2106.14595].

[32] P. D. Nation, M. P. Blencowe, A. J. Rimberg and E. Buks, *Analogue Hawking radiation in a dc-SQUID array transmission line*, Phys. Rev. Lett. **103**, 087004 (2009), doi:10.1103/PhysRevLett.103.087004 [preprint doi:10.48550/arXiv.0904.2589].

[33] H. Katayama, N. Hatakenaka and T. Fujii, *Analogue Hawking radiation from black hole solitons in quantum Josephson transmission lines*, Phys. Rev. D **102**, 086018 (2020), doi:10.1103/PhysRevD.102.086018.

[34] Z. Tian and J. Du, *Analogue Hawking radiation and quantum soliton evaporation in a superconducting circuit*, Eur. Phys. J. C **79**, 994 (2019), doi:10.1140/epjc/s10052-019-7514-9 [preprint doi:10.48550/arXiv.1808.03125].

[35] X.-G. Lan, *Measuring Hawking radiation of a Kerr-Newman black hole in a superconducting transmission line*, Int. J. Theor. Phys. **54**, 116 (2014), doi:10.1007/s10773-014-2207-5.

[36] C. Sabín, *One-dimensional sections of exotic spacetimes with superconducting circuits*, New J. Phys. **20**, 053028 (2018), doi:10.1088/1367-2630/aac0db [preprint doi:10.48550/arXiv.1707.07439].

[37] C. Sabín, *Quantum simulation of traversable wormhole spacetimes in a dc-SQUID array*, Phys. Rev. D **94**, 081501 (2016), doi:10.1103/PhysRevD.94.081501 [preprint doi:10.48550/arXiv.1603.00639].

[38] L. J. Garay, J. R. Anglin, J. I. Cirac and P. Zoller, *Sonic analogue of gravitational black holes in Bose-Einstein condensates*, Phys. Rev. Lett. **85**, 4643 (2000), doi:10.1103/PhysRevLett.85.4643 [preprint doi:10.48550/arXiv.gr-qc/0002015].

[39] L. J. Garay, J. R. Anglin, J. I. Cirac and P. Zoller, *Sonic black holes in dilute Bose-Einstein condensates*, Phys. Rev. A **63**, 023611 (2001), doi:10.1103/PhysRevA.63.023611 [preprint doi:10.48550/arXiv.gr-qc/0005131].

[40] J. Steinhauer, *Observation of self-amplifying Hawking radiation in an analogue black-hole laser*, Nat. Phys. **10**, 864 (2014), doi:10.1038/nphys3104.

[41] J. R. M. de Nova, K. Golubkov, V. I. Kolobov and J. Steinhauer, *Observation of thermal Hawking radiation and its temperature in an analogue black hole*, Nature **569**, 688 (2019), doi:10.1038/s41586-019-1241-0 [preprint doi:10.48550/arXiv.1809.00913].

[42] C. C. H. Ribeiro, S.-S. Baak and U. R. Fischer, *Existence of steady-state black hole analogues in finite quasi-one-dimensional Bose-Einstein condensates*, Phys. Rev. D **105**, 124066 (2022), doi:10.1103/PhysRevD.105.124066 [preprint doi:10.48550/arXiv.2103.05015].

[43] S. J. Robertson, *The theory of Hawking radiation in laboratory analogues*, J. Phys. B: At. Mol. Opt. Phys. **45**, 163001 (2012), doi:10.1088/0953-4075/45/16/163001 [preprint doi:10.48550/arXiv.1508.02569].

[44] T. Jacobson, *Black-hole evaporation and ultrashort distances*, Phys. Rev. D **44**, 1731 (1991), doi:10.1103/PhysRevD.44.1731.

[45] R. Brout, S. Massar, R. Parentani and P. Spindel, *A primer for black hole quantum physics*, Phys. Rep. **260**, 329 (1995), doi:10.1016/0370-1573(95)00008-5.

[46] R. Schützhold and W. G. Unruh, *Hawking radiation in an electromagnetic waveguide?*, Phys. Rev. Lett. **95**, 031301 (2005), doi:10.1103/PhysRevLett.95.031301 [preprint doi:10.48550/arXiv.quant-ph/0408145].

[47] C. C. H. Ribeiro and U. R. Fischer, *Impact of trans-Planckian excitations on black-hole radiation in dipolar condensates*, Phys. Rev. D **107**, L121502 (2023), doi:10.1103/PhysRevD.107.L121502 [preprint doi:10.48550/arXiv.2211.01243].

[48] H. B. Nielsen and M. Ninomiya, *A no-go theorem for regularizing chiral fermions*, Phys. Lett. B **105**, 219 (1981), doi:10.1016/0370-2693(81)91026-1.

[49] F. Arute et al., *Quantum supremacy using a programmable superconducting processor*, Nature **574**, 505 (2019), doi:10.1038/s41586-019-1666-5.

[50] Y. Wu et al., *Strong quantum computational advantage using a superconducting quantum processor*, Phys. Rev. Lett. **127**, 180501 (2021), doi:10.1103/PhysRevLett.127.180501 [preprint doi:10.48550/arXiv.2106.14734].

[51] M. Kjaergaard, M. E. Schwartz, J. Braumüller, P. Krantz, J. I.-J. Wang, S. Gustavsson and W. D. Oliver, *Superconducting qubits: Current state of play*, Annu. Rev. Condens. Matter Phys. **11**, 369 (2020), doi:10.1146/annurev-conmatphys-031119-050605 [preprint doi:10.48550/arXiv.1905.13641].

[52] B. Yurke and J. S. Denker, *Quantum network theory*, Phys. Rev. A **29**, 1419 (1984), doi:10.1103/PhysRevA.29.1419.

[53] G. Burkard, R. H. Koch and D. P. DiVincenzo, *Multilevel quantum description of decoherence in superconducting qubits*, Phys. Rev. B **69**, 064503 (2004), doi:10.1103/PhysRevB.69.064503 [preprint doi:10.48550/arXiv.cond-mat/0308025].

[54] J. Ulrich and F. Hassler, *Dual approach to circuit quantisation using loop charges*, Phys. Rev. B **94**, 094505 (2016), doi:10.1103/PhysRevB.94.094505 [preprint doi:10.48550/arXiv.1605.02750].

[55] U. Vool and M. Devoret, *Introduction to quantum electromagnetic circuits*, Int. J. Circuit Theory Appl. **45**, 897 (2017), doi:10.1002/cta.2359 [preprint doi:10.48550/arXiv.1610.03438].

[56] A. Blais, R.-S. Huang, A. Wallraff, S. M. Girvin and R. J. Schoelkopf, *Cavity quantum electrodynamics for superconducting electrical circuits: An architecture for quantum computation*, Phys. Rev. A **69**, 062320 (2004), doi:10.1103/PhysRevA.69.062320 [preprint doi:10.48550/arXiv.cond-mat/0402216].

[57] A. Blais, J. Gambetta, A. Wallraff, D. I. Schuster, S. M. Girvin, M. H. Devoret and R. J. Schoelkopf, *Quantum-information processing with circuit quantum electrodynamics*, Phys. Rev. A **75**, 032329 (2007), doi:10.1103/PhysRevA.75.032329 [preprint doi:10.48550/arXiv.cond-mat/0612038].

[58] A. Blais, S. M. Girvin and W. D. Oliver, *Quantum information processing and quantum optics with circuit quantum electrodynamics*, Nat. Phys. **16**, 247 (2020), doi:10.1038/s41567-020-0806-z.

[59] A. Blais, A. L. Grimsmo, S. M. Girvin and A. Wallraff, *Circuit quantum electrodynamics*, Rev. Mod. Phys. **93**, 025005 (2021), doi:10.1103/RevModPhys.93.025005 [preprint doi:10.48550/arXiv.2005.12667].

[60] R.-P. Riwar and D. P. DiVincenzo, *Circuit quantisation with time-dependent magnetic fields for realistic geometries*, npj Quantum Inf. **8**, 36 (2022), doi:10.1038/s41534-022-00539-x.

[61] B. Abdo, K. Sliwa, L. Frunzio and M. Devoret, *Directional amplification with a Josephson circuit*, Phys. Rev. X **3**, 031001 (2013), doi:10.1103/PhysRevX.3.031001 [preprint doi:10.48550/arXiv.1302.4663].

[62] A. Kord, D. L. Sounas and A. Alu, *Microwave nonreciprocity*, Proc. IEEE **108**, 1728 (2020), doi:10.1109/JPROC.2020.3006041.

[63] A. Metelmann and A. A. Clerk, *Nonreciprocal photon transmission and amplification via reservoir engineering*, Phys. Rev. X **5**, 021025 (2015), doi:10.1103/PhysRevX.5.021025 [preprint doi:10.48550/arXiv.1502.07274].

[64] A. Metelmann and A. A. Clerk, *Nonreciprocal quantum interactions and devices via autonomous feedforward*, Phys. Rev. A **95**, 013837 (2017), doi:10.1103/PhysRevA.95.013837 [preprint doi:10.48550/arXiv.1610.06621].

[65] B. Tellegen, *The gyrator, a new electric network element*, Philips Res. Rep. **3**, 81 (1948).

[66] G. Viola and D. P. DiVincenzo, *Hall effect gyrators and circulators*, Phys. Rev. X **4**, 021019 (2014), doi:10.1103/PhysRevX.4.021019 [preprint doi:10.48550/arXiv.1312.5190].

[67] M. Rymarz, S. Bosco, A. Ciani and D. P. DiVincenzo, *Hardware-encoding grid states in a nonreciprocal superconducting circuit*, Phys. Rev. X **11**, 011032 (2021), doi:10.1103/PhysRevX.11.011032 [preprint doi:10.48550/arXiv.2002.07718].

[68] L.-A. Sellem, A. Sarlette, Z. Leghtas, M. Mirrahimi, P. Rouchon and P. Campagne-Ibarcq, *Dissipative protection of a GKP qubit in a high-impedance superconducting circuit driven by a microwave frequency comb*, Phys. Rev. X **15**, 011011 (2025), doi:10.1103/PhysRevX.15.011011 [preprint doi:10.48550/arXiv.2304.01425].

[69] P. Virtanen and T. T. Heikkilä, *Nonreciprocal Josephson linear response*, Phys. Rev. Lett. **132**, 046002 (2024), doi:10.1103/PhysRevLett.132.046002 [preprint doi:10.48550/arXiv.2306.12295].

[70] R. -P. Riwar, *Discrete control of capacitance in quantum circuits*, (arXiv preprint) doi:10.48550/arXiv.2306.00587.

[71] F. J. Matute-Cañadas, L. Tosi and A. L. Yeyati, *Quantum circuits with multiterminal Josephson-Andreev junctions*, PRX Quantum **5**, 020340 (2024), doi:10.1103/PRXQuantum.5.020340 [preprint doi:10.48550/arXiv.2312.17305].

[72] O. Kashuba, R. Mummadavarapu and R. -P. Riwar, *Of gyrators and anyons*, (arXiv preprint) doi:10.48550/arXiv.2410.20835.

[73] R.-P. Riwar, M. Houzet, J. S. Meyer and Y. V. Nazarov, *Multi-terminal Josephson junctions as topological matter*, Nat. Commun. **7**, 11167 (2016), doi:10.1038/ncomms11167 [preprint doi:10.48550/arXiv.1503.06862].

[74] V. Fatemi, A. R. Akhmerov and L. Bretheau, *Weyl Josephson circuits*, Phys. Rev. Res. **3**, 013288 (2021), doi:10.1103/PhysRevResearch.3.013288 [preprint doi:10.48550/arXiv.2008.13758].

[75] L. Peyruchat, J. Griesmar, J.-D. Pillet and Ç. Ö. Girit, *Transconductance quantisation in a topological Josephson tunnel junction circuit*, Phys. Rev. Res. **3**, 013289 (2021), doi:10.1103/PhysRevResearch.3.013289 [preprint doi:10.48550/arXiv.2009.03291].

[76] H. Weisbrich, R. L. Klees, G. Rastelli and W. Belzig, *Second Chern number and non-Abelian Berry phase in topological superconducting systems*, PRX Quantum **2**, 010310 (2021), doi:10.1103/PRXQuantum.2.010310 [preprint doi:10.48550/arXiv.2008.08319].

[77] R. L. Klees, J. C. Cuevas, W. Belzig and G. Rastelli, *Ground-state quantum geometry in superconductor–quantum dot chains*, Phys. Rev. B **103**, 014516 (2021), doi:10.1103/PhysRevB.103.014516 [preprint doi:10.48550/arXiv.2009.11768].

[78] L. Teshler, H. Weisbrich, J. Sturm, R. L. Klees, G. Rastelli and W. Belzig, *Ground state topology of a four-terminal superconducting double quantum dot*, SciPost Phys. **15**, 214 (2023), doi:10.21468/SciPostPhys.15.5.214 [preprint doi:10.48550/arXiv.2304.11982].

[79] T. Herrig and R.-P. Riwar, *Cooper-pair transistor as a minimal topological quantum circuit*, Phys. Rev. Res. **4**, 013038 (2022), doi:10.1103/PhysRevResearch.4.013038 [preprint doi:10.48550/arXiv.2012.10655].

[80] L. Peyruchat, R. H. Rodriguez, J.-L. Smirr, R. Leone and Ç. Ö. Girit, *Spectral signatures of nontrivial topology in a superconducting circuit*, Phys. Rev. X **14**, 041041 (2024), doi:10.1103/PhysRevX.14.041041 [preprint doi:10.48550/arXiv.2401.10876].

[81] W. Jung, S. Jin, S. Park, S.-H. Shin, K. Watanabe, T. Taniguchi, G. Y. Cho and G.-H. Lee, *Full tomography of topological Andreev bands in graphene Josephson junctions*, (arXiv preprint) doi:10.48550/arXiv.2411.01170.

[82] Y. S. Kivshar and B. A. Malomed, *Dynamics of solitons in nearly integrable systems*, Rev. Mod. Phys. **61**, 763 (1989), doi:10.1103/RevModPhys.61.763.

[83] A. V. Ustinov, *Solitons in Josephson junctions*, Phys. D: Nonlinear Phenom. **123**, 315 (1998), doi:10.1016/S0167-2789(98)00131-6.

[84] A. Wallraff, A. V. Ustinov, V. V. Kurin, I. A. Shereshevsky and N. K. Vdovicheva, *Whispering vortices*, Phys. Rev. Lett. **84**, 151 (2000), doi:10.1103/PhysRevLett.84.151 [preprint doi:10.48550/arXiv.cond-mat/9911260].

[85] R. Fazio, *Quantum phase transitions and vortex dynamics in superconducting networks*, Phys. Rep. **355**, 235 (2001), doi:10.1016/S0370-1573(01)00022-9.

[86] J. Cho, D. G. Angelakis and S. Bose, *Fractional quantum Hall state in coupled cavities*, Phys. Rev. Lett. **101**, 246809 (2008), doi:10.1103/PhysRevLett.101.246809.

[87] S. Gladchenko, D. Olaya, E. Dupont-Ferrier, B. Douçot, L. B. Ioffe and M. E. Gershenson, *Superconducting nanocircuits for topologically protected qubits*, Nat. Phys. **5**, 48 (2008), doi:10.1038/nphys1151.

[88] B. M. Terhal, F. Hassler and D. P. DiVincenzo, *From Majorana fermions to topological order*, Phys. Rev. Lett. **108**, 260504 (2012), doi:10.1103/PhysRevLett.108.260504.

[89] A. A. Houck, H. E. Türeci and J. Koch, *On-chip quantum simulation with superconducting circuits*, Nat. Phys. **8**, 292 (2012), doi:10.1038/nphys2251.

[90] M. Houzet and L. I. Glazman, *Microwave spectroscopy of a weakly pinned charge density wave in a superinductor*, Phys. Rev. Lett. **122**, 237701 (2019), doi:10.1103/PhysRevLett.122.237701.

[91] N. A. Olekhno, A. D. Rozenblit, A. A. Stepanenko, A. A. Dmitriev, D. A. Bobylev and M. A. Gorlach, *Topological transitions driven by quantum statistics and their electrical circuit emulation*, Phys. Rev. B **105**, 205113 (2022), doi:10.1103/PhysRevB.105.205113.

[92] M. M. Wauters, L. Maffi and M. Burrello, *Engineering a Josephson junction chain for the simulation of the quantum clock model*, Phys. Rev. B **111**, 045418 (2025), doi:10.1103/PhysRevB.111.045418.

[93] E. Flurin, N. Roch, F. Mallet, M. H. Devoret and B. Huard, *Generating entangled microwave radiation over two transmission lines*, Phys. Rev. Lett. **109**, 183901 (2012), doi:10.1103/PhysRevLett.109.183901.

[94] C. M. Wilson, G. Johansson, A. Pourkabirian, M. Simoen, J. R. Johansson, T. Duty, F. Nori and P. Delsing, *Observation of the dynamical Casimir effect in a superconducting circuit*, Nature **479**, 376 (2011), doi:10.1038/nature10561.

[95] H. Katayama, S. Ishizaka, N. Hatakenaka and T. Fujii, *Solitonic black holes induced by magnetic solitons in a dc-SQUID array transmission line coupled with a magnetic chain*, Phys. Rev. D **103**, 066025 (2021), doi:10.1103/PhysRevD.103.066025.

[96] H. Katayama, *Designed analogue black hole solitons in Josephson transmission lines*, IEEE Trans. Appl. Supercond. **31**, 1 (2021), doi:10.1109/TASC.2021.3058076.

[97] H. Katayama, *Quantum-circuit black hole lasers*, Sci. Rep. **11**, 19137 (2021), doi:10.1038/s41598-021-98456-0.

[98] H. Katayama, N. Hatakenaka, T. Fujii and M. P. Blencowe, *Analogue black-white hole solitons in traveling wave parametric amplifiers with superconducting nonlinear asymmetric inductive elements*, Phys. Rev. Res. **5**, L022055 (2023), doi:10.1103/PhysRevResearch.5.L022055.

[99] X. You, J. A. Sauls and J. Koch, *Circuit quantisation in the presence of time-dependent external flux*, Phys. Rev. B **99**, 174512 (2019), doi:10.1103/PhysRevB.99.174512.

[100] S. Pal and C. Benjamin, *Tuning the* $0-\pi$ *Josephson junction with a magnetic impurity: Role of tunnel contacts, exchange coupling,* $e-e$ *interactions and high-spin states*, Sci. Rep. **8**, 5208 (2018), doi:10.1038/s41598-018-23517-w.

[101] C. Li, B. de Ronde, J. de Boer, J. Ridderbos, F. Zwanenburg, Y. Huang, A. Golubov and A. Brinkman, *Zeeman-effect-induced* $0-\pi$ *transitions in ballistic Dirac semimetal Josephson junctions*, Phys. Rev. Lett. **123**, 026802 (2019), doi:10.1103/PhysRevLett.123.026802.

[102] C. T. Ke et al., *Ballistic superconductivity and tunable π–junctions in InSb quantum wells*, Nat. Commun. **10**, 3764 (2019), doi:10.1038/s41467-019-11742-4.

[103] W. D. Heiss, *Exceptional points of non-Hermitian operators*, J. Phys. A: Math. Gen. **37**, 2455 (2004), doi:10.1088/0305-4470/37/6/034.

[104] A. V. Hlushchenko, D. V. Novitsky, V. I. Shcherbinin and V. R. Tuz, *Multimode $\mathcal{PT}$-symmetry thresholds and third-order exceptional points in coupled dielectric waveguides with loss and gain*, J. Opt. **23**, 125002 (2021), doi:10.1088/2040-8986/ac31d4.

[105] S. Xia, C. Danieli, Y. Zhang, X. Zhao, H. Lu, L. Tang, D. Li, D. Song and Z. Chen, *Higher-order exceptional point and Landau–Zener Bloch oscillations in driven non-Hermitian photonic Lieb lattices*, APL Photonics **6**, 126106 (2021), doi:10.1063/5.0069633.

[106] K. Ding, G. Ma, Z. Q. Zhang and C. T. Chan, *Experimental demonstration of an anisotropic exceptional point*, Phys. Rev. Lett. **121**, 085702 (2018), doi:10.1103/PhysRevLett.121.085702.

[107] F. E. Öztürk, T. Lappe, G. Hellmann, J. Schmitt, J. Klaers, F. Vewinger, J. Kroha and M. Weitz, *Observation of a non-Hermitian phase transition in an optical quantum gas*, Science **372**, 88 (2021), doi:10.1126/science.abe9869.

[108] Q. Liao, C. Leblanc, J. Ren, F. Li, Y. Li, D. Solnyshkov, G. Malpuech, J. Yao and H. Fu, *Experimental measurement of the divergent quantum metric of an exceptional point*, Phys. Rev. Lett. **127**, 107402 (2021), doi:10.1103/PhysRevLett.127.107402.

[109] W. D. Heiss, *The physics of exceptional points*, J. Phys. A: Math. Theor. **45**, 444016 (2012), doi:10.1088/1751-8113/45/44/444016.

[110] H. C. Wu, L. Jin and Z. Song, *Inversion symmetric non-Hermitian Chern insulator*, Phys. Rev. B **100**, 155117 (2019), doi:10.1103/PhysRevB.100.155117.

[111] I. Mandal and E. J. Bergholtz, *Symmetry and higher-order exceptional points*, Phys. Rev. Lett. **127**, 186601 (2021), doi:10.1103/PhysRevLett.127.186601.

[112] P. San-Jose, J. Cayao, E. Prada and R. Aguado, *Majorana bound states from exceptional points in non-topological superconductors*, Sci. Rep. **6**, 21427 (2016), doi:10.1038/srep21427.

[113] K. Ding, C. Fang and G. Ma, *Non-Hermitian topology and exceptional-point geometries*, Nat. Rev. Phys. **4**, 745 (2022), doi:10.1038/s42254-022-00516-5.

[114] F. K. Kunst, E. Edvardsson, J. C. Budich and E. J. Bergholtz, *Biorthogonal bulk-boundary correspondence in non-Hermitian systems*, Phys. Rev. Lett. **121**, 026808 (2018), doi:10.1103/PhysRevLett.121.026808.

[115] K. Kawabata, K. Shiozaki, M. Ueda and M. Sato, *Symmetry and topology in non-Hermitian physics*, Phys. Rev. X **9**, 041015 (2019), doi:10.1103/PhysRevX.9.041015.

[116] E. J. Bergholtz, J. C. Budich and F. K. Kunst, *Exceptional topology of non-Hermitian systems*, Rev. Mod. Phys. **93**, 015005 (2021), doi:10.1103/RevModPhys.93.015005.

[117] J. Avila, F. Peñaranda, E. Prada, P. San-Jose and R. Aguado, *Non-Hermitian topology as a unifying framework for the Andreev versus Majorana states controversy*, Commun. Phys. **2**, 133 (2019), doi:10.1038/s42005-019-0231-8.

[118] W. C. Smith, A. Kou, X. Xiao, U. Vool and M. H. Devoret, *Superconducting circuit protected by two-Cooper-pair tunneling*, npj Quantum Inf. **6**, 8 (2020), doi:10.1038/s41534-019-0231-2.

[119] W. C. Smith, M. Villiers, A. Marquet, J. Palomo, M. R. Delbecq, T. Kontos, P. Campagne-Ibarcq, B. Douçot and Z. Leghtas, *Magnifying quantum phase fluctuations with Cooper-pair pairing*, Phys. Rev. X **12**, 021002 (2022), doi:10.1103/PhysRevX.12.021002.

[120] L. Banszerus, C. W. Andersson, W. Marshall, T. Lindemann, M. J. Manfra, C. M. Marcus and S. Vaitiekėnas, *Hybrid Josephson rhombus: A superconducting element with tailored current-phase relation*, Phys. Rev. X **15**, 011021 (2025), doi:10.1103/PhysRevX.15.011021 [preprint doi:10.48550/arXiv.2406.20082].

[121] Y. Nakamura, M. Mine, M. Okumura and Y. Yamanaka, *Condition for emergence of complex eigenvalues in the Bogoliubov–de Gennes equations*, Phys. Rev. A **77**, 043601 (2008), doi:10.1103/PhysRevA.77.043601.

[122] M. Mine, M. Okumura, T. Sunaga and Y. Yamanaka, *Quantum field theoretical description of unstable behavior of trapped Bose–Einstein condensates with complex eigenvalues of Bogoliubov–de Gennes equations*, Ann. Phys. **322**, 2327 (2007), doi:10.1016/j.aop.2007.01.008.

[123] N. W. Ashcroft and N. D. Mermin, *Solid state physics*, Cengage Learning, Boston, USA, ISBN 9780030839931 (1976).

[124] F. D. M. Haldane, *'Luttinger liquid theory' of one-dimensional quantum fluids. I. Properties of the Luttinger model and their extension to the general 1D interacting spinless Fermi gas*, J. Phys. C: Solid State Phys. **14**, 2585 (1981), doi:10.1088/0022-3719/14/19/010.

[125] A. Recati, N. Pavloff and I. Carusotto, *Bogoliubov theory of acoustic Hawking radiation in Bose-Einstein condensates*, Phys. Rev. A **80**, 043603 (2009), doi:10.1103/PhysRevA.80.043603.

[126] J. Curtis, G. Refael and V. Galitski, *Evanescent modes and step-like acoustic black holes*, Ann. Phys. **407**, 148 (2019), doi:10.1016/j.aop.2019.04.017.

[127] P. T. Nam, M. Napiórkowski and J. P. Solovej, *Diagonalization of bosonic quadratic Hamiltonians by Bogoliubov transformations*, J. Funct. Anal. **270**, 4340 (2016), doi:10.1016/j.jfa.2015.12.007.

[128] I. C. Rodrigues, G. A. Steele and D. Bothner, *Photon pressure with an effective negative mass microwave mode*, Phys. Rev. Lett. **132**, 203603 (2024), doi:10.1103/PhysRevLett.132.203603.

[129] F. Fani Sani, I. C. Rodrigues, D. Bothner and G. A. Steele, *Level attraction and idler resonance in a strongly driven Josephson cavity*, Phys. Rev. Res. **3**, 043111 (2021), doi:10.1103/PhysRevResearch.3.043111.

[130] G. E. Volovik, *Black hole and Hawking radiation by type-II Weyl fermions*, J. Exp. Theor. Phys. Lett. **104**, 645 (2016), doi:10.1134/S0021364016210050.

[131] W. A. Little, *Possibility of synthesizing an organic superconductor*, Phys. Rev. **134**, A1416 (1964), doi:10.1103/PhysRev.134.A1416.

[132] R. Landauer, *Can capacitance be negative?*, Collect. Phenom. **2**, 167 (1976).

[133] G. Catalan, D. Jiménez and A. Gruverman, *Negative capacitance detected*, Nat. Mater. **14**, 137 (2015), doi:10.1038/nmat4195.

[134] P. Zubko, J. C. Wojdeł, M. Hadjimichael, S. Fernandez-Pena, A. Sené, I. Luk'yanchuk, J.-M. Triscone and J. Íñiguez, *Negative capacitance in multidomain ferroelectric superlattices*, Nature **534**, 524 (2016), doi:10.1038/nature17659.

[135] M. Hoffmann, A. I. Khan, C. Serrao, Z. Lu, S. Salahuddin, M. Pešić, S. Slesazeck, U. Schroeder and T. Mikolajick, *Ferroelectric negative capacitance domain dynamics*, J. Appl. Phys. **123**, 184101 (2018), doi:10.1063/1.5030072.

[136] M. Hoffmann, S. Slesazeck, U. Schroeder and T. Mikolajick, *What's next for negative capacitance electronics?*, Nat. Electron. **3**, 504 (2020), doi:10.1038/s41928-020-00474-9.

[137] A. Hamo, A. Benyamini, I. Shapir, I. Khivrich, J. Waissman, K. Kaasbjerg, Y. Oreg, F. von Oppen and S. Ilani, *Electron attraction mediated by Coulomb repulsion*, Nature **535**, 395 (2016), doi:10.1038/nature18639.

[138] B. A. Placke, T. Pluecker, J. Splettstoesser and M. R. Wegewijs, *Attractive and driven interactions in quantum dots: Mechanisms for geometric pumping*, Phys. Rev. B **98**, 085307 (2018), doi:10.1103/PhysRevB.98.085307.

[139] T. Herrig, J. H. Pixley, E. J. König and R.-P. Riwar, *Quasiperiodic circuit quantum electrodynamics*, npj Quantum Inf. **9**, 116 (2023), doi:10.1038/s41534-023-00786-6.

[140] T. Herrig, C. Koliofoti, J. H. Pixley, E. J. König and R.-P. Riwar, *Emulating moiré materials with quasiperiodic circuit quantum electrodynamics*, Phys. Rev. B **111**, L201104 (2025), doi:10.1103/PhysRevB.111.L201104 [preprint doi:10.48550/arXiv.2310.15103].

[141] C. Koliofoti and R.-P. Riwar, *Compact description of quantum phase slip junctions*, npj Quantum Inf. **9**, 125 (2023), doi:10.1038/s41534-023-00790-w.

[142] R.-P. Riwar, *Charge quantisation and detector resolution*, SciPost Phys. **10**, 093 (2021), doi:10.21468/SciPostPhys.10.4.093.

[143] A. Anferov, S. P. Harvey, F. Wan, J. Simon and D. I. Schuster, *Superconducting qubits above 20 GHz operating over 200 mK*, PRX Quantum **5**, 030347 (2024), doi:10.1103/PRXQuantum.5.030347 [preprint doi:10.48550/arXiv.2402.03031].

[144] R. Balbinot, A. Fabbri, S. Fagnocchi, A. Recati and I. Carusotto, *Nonlocal density correlations as a signature of Hawking radiation from acoustic black holes*, Phys. Rev. A **78**, 021603 (2008), doi:10.1103/PhysRevA.78.021603.

[145] I. Klich, *Full counting statistics: An elementary derivation of Levitov's formula*, (arXiv preprint) doi:10.48550/arXiv.cond-mat/0209642.

[146] S. Kim and F. Hassler, *Third quantisation for bosons: Symplectic diagonalisation, non-Hermitian Hamiltonian, and symmetries*, J. Phys. A: Math. Theor. **56**, 385303 (2023), doi:10.1088/1751-8121/acf177.

[147] T. Prosen, *Third quantisation: A general method to solve master equations for quadratic open Fermi systems*, New J. Phys. **10**, 043026 (2008), doi:10.1088/1367-2630/10/4/043026.